

Mesh Silksong: Auto-Regressive Mesh Generation as Weaving Silk

Gaochao Song¹ Zibo Zhao² Haohan Weng² Jingbo Zeng¹
Rongfei Jia^{3*} Shenghua Gao^{1†}

¹University of Hong Kong, ²Tencent Hunyuan 3D, ³Math Magic
<https://gaochao-s.github.io/pages/MeshSilksong/>



Figure 1: Meshes generated by **Mesh Silksong**. Vertices are colored based on different connected component of mesh. Our method is connected component aware based on special tokens when generating, which helps capture small but critical parts of mesh.

Abstract

We introduce Mesh Silksong, a compact and efficient mesh representation tailored to generate the polygon mesh in an auto-regressive manner akin to silk weaving. Existing mesh tokenization methods always produce token sequences with repeated vertex tokens, wasting the network capability. Therefore, our approach tokenizes mesh vertices by accessing each mesh vertice only once, reduces the token sequence’s redundancy by 50%, and achieves a state-of-the-art compression rate of approximately 22%. Furthermore, Mesh Silksong produces polygon meshes with superior geometric properties, including manifold topology, watertight detection, and consistent face normals, which are critical for practical applications. Experimental results demonstrate the effectiveness of our approach, showcasing not only intricate mesh generation but also significantly improved geometric integrity.

*This work is strongly supported by Math Magic.

[†]Corresponding author.

1 Introduction

The polygon mesh is a fundamental representation of 3D assets and is extensively utilized in video games, film production, and virtual reality. Generating high-quality meshes can significantly reduce the workload of artists and improve industrial efficiency. Recent advancements [29; 2; 31; 38; 19; 47] have focused on leveraging autoregressive models to produce high-quality polygon meshes by directly learning vertex distributions and topological connectivity from handcrafted meshes. Such approaches have yielded promising results with superior mesh topology structures preserved.

The core of auto-regressive mesh generation lies in designing an effective token representation for meshes that fully leverages the powerful generative capabilities of autoregressive models. However, mesh-to-token conversion imposes higher demands on geometric processing algorithms. Given the inherent instability of autoregressive models, a key challenge is effectively compressing the information in meshes while preserving their topological structures, such as manifold topology, watertightness, and surface normal consistency.

Current efficient mesh-to-token conversion algorithms can be broadly divided into two categories: tree-traversal-based (e.g., EdgeRunner [31] and TreeMeshGPT [19]) and local patch-based (e.g., BPT [38], Nautilus [36], and DeepMesh [47]). Tree-traversal methods leverage the half-edge data structure to preserve manifold topology but suffer from error accumulation during triangle traversal, leading to instability in mesh generation. In contrast, local patch methods generate more stable meshes by treating local triangle patches independently. However, these meshes are often non-manifold, making them less suitable for applications like UV unwrapping, 3D printing, and physical simulations.

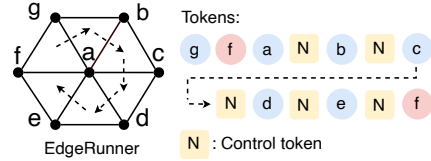


Figure 2: Illustration mesh compression method used in EdgeRunner [31]. The starting vertex f is encoded twice, resulting in a redundant token sequence.

In addition, approaches in both categories face the following limitations:

- **Redundant Vertex Compression:** Fig. 2 shows that when traversing vertices along a non-boundary vertex a , the starting vertex f is encoded twice. This redundancy occurs universally for non-boundary vertices to avoid missing adjacent triangles, with similar issues observed in BPT [38], TreeMeshGPT [19], MeshAnythingv2 [3], etc.
- **Lacking Global Structure Awareness:** All triangles are treated equally during generation, causing the model to overlook small but critical components, such as eyes formed by only a few triangles, as shown in lines 2,6 of Fig. 6.

To address these issues, we propose a novel mesh tokenization algorithm. We classify vertices into several layers based on the graph distance to a given start vertex, sort them per layer, and calculate the layer adjacency matrices based on the layered and sorted vertices to encode the topology. Then, vertex tokens and topology tokens compressed from adjacency matrices are organized into a unified format for mesh representation. Compared to the existing methods [31; 38; 19], our approach compresses each vertex only once, reducing approximately 50% of redundant vertex information. By combining our method with the block-wise indexing proposed in BPT [38] (reducing from 3 tokens per vertex to 2 tokens per vertex), the final compression ratio improves from 0.26 (BPT) to 0.22, enabling more efficient mesh compression and allowing the representation of finer geometric details within the same token length. Further, our method is sensitive to the connected components of the mesh since the algorithm operates on connected components separately and utilizes special tokens for marking. This guides the generative model to focus on the overall geometric topology and effectively captures small, often overlooked connected components. As a manifold-based mesh representation, our approach strongly supports watertightness detection and imposes robust constraints on surface normal consistency, showcasing excellent geometric properties.

In summary, our contributions are as follows:

- We present a novel and efficient mesh tokenization approach that reduces 50% of redundant vertex information compared to existing methods, improving the compression ratio from 0.26 (BPT [38]) to 0.22.

- Our manifold-based mesh representation demonstrates excellent geometric properties, including support for watertightness detection and constraints on surface normal consistency.
- Experimental results validate the effectiveness of our approach, highlighting its ability to capture small but critical connected components and improve overall geometric quality.

2 Related Work

2.1 3D Mesh Generation

With the success of 2D generation [26], 3D generation has emerged as a popular research direction. Initially, SDS-based optimization methods [6; 16; 18; 32; 25; 44] were employed to address the scarcity of 3D datasets, followed by subsequent works [28; 43] aimed at resolving the Janus problem. As 3D datasets have expanded [8; 7], feed-forward 3D generation methods [12; 15; 41] have seen significant advancements. While these approaches greatly enhance generation speed, they suffer from low-quality meshes and limited diversity. More recent methods [5; 17; 35; 39; 40; 42; 48; 45; 46; 13] focus on learning compressed 3D representations via VAEs combined with latent diffusion models. However, above methods typically rely on voxels or SDFs to represent 3d shape, and then translate object to dense triangle meshes using algorithms like Marching Cubes [20]. This process frequently results in subpar geometric topology, characterized by poorly structured or cluttered wireframes.

2.2 Auto-Regressive Based Mesh Generation

To generate meshes with high quality topology, recent methods leverage autoregressive models to learn vertex distributions and connections directly from handcrafted meshes. MeshGPT [29] pioneered this approach by encoding meshes into tokens using VQ-VAE[34], enabling direct supervision from handcrafted data. MeshXL [2] identified that quantizing triangle vertex tokens without trainable VQ-VAE is key to scaling datasets. Following this, MeshAnything v2 [4] and EdgeRunner [31] introduced compact tokenization algorithms, increasing the maximum face count from 800 [3] to 1.6k and 4k, respectively. BPT [38] and TreeMeshGPT [19] further optimized both geometry compression and vertex compression supporting 5k-8k faces. For autoregressive model optimization, Meshtron [11] proposed an hourglass transformer [22] and truncation training, enabling up to 16k face generation. LLaMAMesh [37] leveraged pretrained LLMs for text-to-mesh generation, while DeepMesh [47] applied reinforcement learning via Direct Preference Optimization (DPO) [24], significantly improving mesh aesthetics.

3 Method

Our mesh tokenization algorithm consists of the following steps: (1) Preprocessing: We developed a lightweight, non-manifold edge processing algorithm to ensure that the input meshes strictly adhere to manifold topology requirements. (2) Vertex Layering and Sorting: Starting from a given half-edge, all vertices are classified into multiple layers resembling contour lines and are subsequently sorted based on their local order. (3) Layer Adjacency Matrices Compression: Two-layer adjacency matrices are computed for each layer and then compressed into tokens. (4) Token Packing: Vertex tokens and their corresponding topology tokens (compressed from layer adjacency matrices) are organized into a unified format optimized for an auto-regressive generation.

3.1 Non-manifold Edges Processing

The non-manifold edges for a mesh refer to the edges shared by 3 or more faces. As illustrated in Fig. 3, the edge 9-10 is non-manifold edge since it is shared by triangle 9-10-11, 9-10-8 and 9-4-10. A naive way to eliminate it, as done in EdgeRunner [14], is to re-traverse all of the triangle edges and mark the third-occurring edge as bounding edge. However, this may cause several results depending on the order in which the triangles appear. As shown in (b) and (c) of Fig. 3, though both of the results indicate the non-manifold edges are eliminated, the latter destroyed the completeness of mesh surface which is not friendly for our following steps. To solve this, we transform this problem into an equivalent edge graph partition question. In our definition, the vertex i 's edge graph \mathcal{G}_i indicates an undirected graph formed by all of the faces including the vertex. As shown in (d) of Fig.

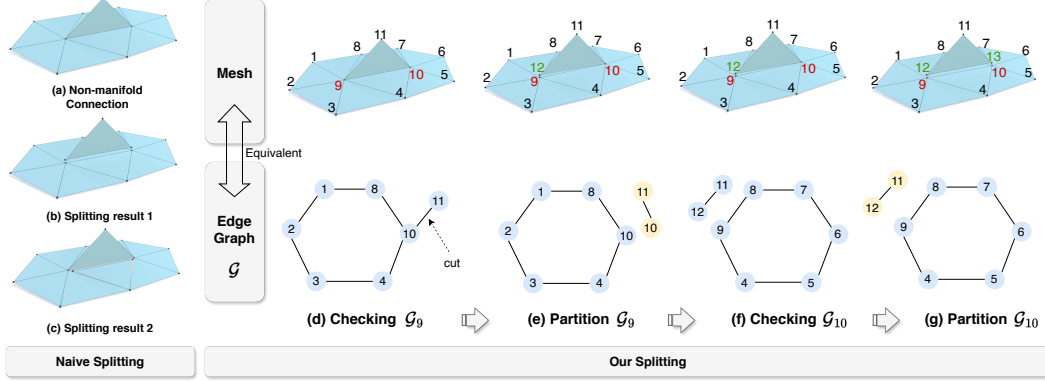


Figure 3: Illustration of non-manifold edge processing. Naive non-manifold edge splitting will result (b) or (c) since triangles associated with non-manifold edges are indeterminate, while the latter compromised the integrity of surface. Our algorithm keeps the integrity of local surface.

3, the "nodes" in edge graph \mathcal{G}_9 represent the edges connected to reference vertex 9 in mesh, while the "edges" in edge graph represent the faces in mesh, which are formed by the "nodes" and reference vertex 9. To guarantee manifold structure for mesh, the edge graph of each mesh vertex should be either a cycle or a chain without any branch, as well as having only one connected component. The whole algorithm is illustrated in (d)-(g) of Fig. 3, after checking \mathcal{G}_9 , the branched "edge" 10-11 (indicating the face 9-10-11 of mesh) is easily detected and will be detached from the cycle. Then at (e), we exclude the isolated connected component 10-11 from edge graph, which is equivalent to detach face 9-10-11 from vertex 9 in mesh, and register a new vertex 12 for mesh edge 10-11. After (e), notice the edge graph of \mathcal{G}_{10} will also be updated. Then (f) will start for checking \mathcal{G}_{10} and so on. The algorithm proceeds along all of the non-manifold points with BFS traversal and updates edge graph for each vertex dynamically. More complex details are presented in Appendix A.

3.2 Vertices Layering and Sorting

As shown in Fig. 5, given a manifold mesh \mathcal{M} and a start half-edge, all vertices \mathcal{V} can be assigned a unique coordinate (L, i) , and we denote the vertex as \mathcal{V}_i^L . The two vertices of start half-edge are marked as $\mathcal{V}_1^0, \mathcal{V}_1^1$. The L , denoted as layer number, represents the shortest path to the initial vertex \mathcal{V}_1^0 along the edges of \mathcal{M} , which is easily obtained by BFS traversal. The i , denoted as the layer order, represents the order of the vertices in the same layer L , which can be obtained based on the local order of vertices in layer $L - 1$. Take Fig. 4 as an example, for vertex a of layer L , the neighbor vertices firstly can be arranged counterclockwise based on half-edge data structure, hence the 3 vertices' order (g, h, b) for layer $L + 1$ is decided. Further, given all of the sorted vertices of layer L , the order of all vertices in layer $L + 1$ can be decided in such a manner. Notice the start half edge $\mathcal{V}_1^0 - \mathcal{V}_1^1$ of mesh is given, the sequence of the sorted vertices on each layer can be determined one by one. In practice, we sort all of the half-edges of given mesh in the order of y - z - x and select the smallest one as start half-edge.

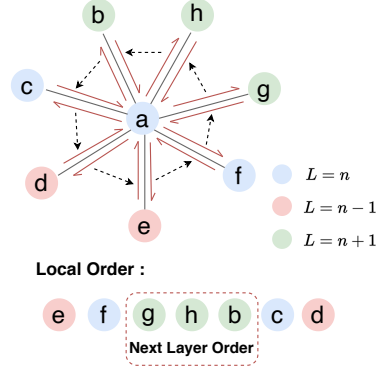


Figure 4: The counterclockwise order of neighbor vertices for vertex a is easily obtained via half-edge data structure. Hence the next layer vertices' order are decided.

3.3 Layer Adjacency Matrices Compression

After vertex layering and sorting, the connection of mesh vertices are classified to the following 2 situations: self-layer connection or between-layer connection. The self-layer connection refers to the connected two vertices belongs to the same layer L , while the between-layer connection refers to the connected vertices belongs to different layer $L, L - 1$. Therefore, given vertices of layer L , we describe the related topology connection via two adjacency matrices named Self-Layer Matrix \mathcal{S}_L

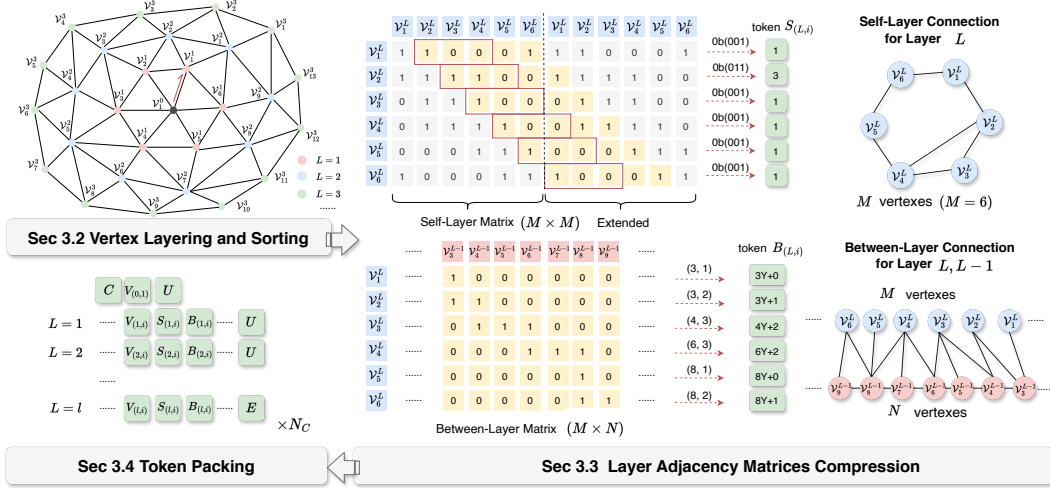


Figure 5: Illustration of our mesh tokenization algorithm. The mesh vertex for layer L with order i is denoted as v_i^L , its corresponding three types of tokens are denoted as $V_{(L,i)}$, $S_{(L,i)}$, $B_{(L,i)}$, coming from vertex coordinate quantization, self-layer matrix S_L 's compression and between-layer matrix B_L 's compression respectively. The index (i, j) for self-layer matrix S_L indicates the connection of v_i^L, v_j^L , while the index (i, j) for between-layer matrix B_L indicates the connection of v_i^L, v_j^{L-1} .

and Between-Layer Matrix B_L . In the next part, we will describe how to transform the matrices to tokens to compress the topology information of a mesh.

Self-Layer Matrix Compression. As illustrated in Fig. 5, the Self-Layer Matrix S_L is a 0-1 symmetric matrix with shape $M \times M$, where M represents the vertex number for layer L . The goal is to compress the M rows of matrix to M tokens, where we denote the token index for row i as $S_{(L,i)}$. A easy way to compress S_L is directly apply binary coding for every row, however, the word table for tokens would be 2^m , where m represents the max number of vertices for all of the layers. Such a large word table is unacceptable, however, the sparsity of the matrix provides clues for efficient compression. Firstly, we extend the symmetric matrix to $M \times 2M$, noticing the row (i, i) of matrix is useless, the valid value number for every row is $M - 1$, as denoted as yellow block 0, 1 in Fig. 5. Secondly, a window with size W (denoted as red box in figure with $W=3$) is located from row $(i, i+1)$ to $(i, i+1+W)$ to compute the binary coding since we notice the self-layer connection tends to occur at adjacent vertices.

In practice, the W is set to 8 and the window will not slide since there usually will not appear "1" outside the window. In Fig. 5, the "1" outside the window at the position like (1, 6) is actually repeated to the "1" at (6, 7), which is removed in practice. The initial word table size for self-layer matrix is 2^W . For some special situation that "1" appears outside the window, we extend the word table size to $2^W + m$ to handle this, please refer to Appendix B for details.

Between-Layer Matrix Compression. As illustrated in Fig. 5, the Between-Layer Matrix is a 0-1 matrix with size $M \times N$, where M is the number of vertices for layer L and N is the number of vertices for layer $L-1$. Considering the connection rule is different from self-layer matrix, another way is applied to compress it. We notice the "1" tends to appear continuously for each row. For example, there are continuous three "1"s at (3, 4), (3, 5), (3, 6) for row 3, hence we firstly mark row 3 as $(x, y) = (4, 3)$, where $x \in [1, m]$ represents the start column index of "1" and $y \in [1, Y]$ represents the number of continuous "1"s where Y is a predefined number of max continuous "1"s. Then the token index for $B_{(L,i)}$ should be $x \cdot Y + y - 1$. For the simplified situation, as shown in Fig. 5, the word table size for between-layer matrix is $m \cdot Y$.

In practice, the "1"s will appear continuously twice or even more, we transform this problem to a equivalent Stars and Bars question, and the actual word table size is:

$$m \cdot (2 \cdot W' + 2 \cdot C_{W'-1}^2 + C_{W'-1}^3)$$

where W' is a predefined window size for between-layer matrix, see Appendix C for more details.

3.4 Token Packing and Model

Token Packing. For M vertices in layer L , we now have three types of tokens: vertex tokens $V_{(L,i)}$ and topology tokens $S_{(L,i)}, B_{(L,i)}$ derived from matrix compression. The vertex tokens compressed vertex's position and usually contain 3 sub-tokens representing quantized x - y - z coordinate. In BPT [38], the sub-token number is decreased to 2 to represent 128 bit quantized mesh, and we follow this representation in our method. The two topology tokens $S_{(L,i)}, B_{(L,i)}$ usually contain one sub-token each other. To obtain the full sequence for training, as illustrated in Fig. 5, we start from token **C**, which represents a connected component of mesh (If mesh has N_C connected components, there will be N_C **C** tokens and algorithm of Sec. 3.2, Sec. 3.3 will perform totally N_C times on each connected components). We pack $V_{(L,i)}, S_{(L,i)}, B_{(L,i)}$ together for vertex \mathcal{V}_i^L and arrange different vertex's tokens following the layer order. The vertex token for \mathcal{V}_1^0 is placed at first and has no topology tokens. Tokens for each layer is separated with an "up-layer" control token **U** and the last one is replaced by another control token **E** to represent the end of connected component.

Model Architecture. The core model we use for training is a decoder-only transformer, each layer contains a cross-attention and a self-attention layer with a feed-forward network. For point cloud conditioned generation, the point cloud feature is extracted from Michelangelo [49] and injected to auto-regressive model via cross-attention. The Michelangelo and core model are trained jointly.

Training Strategy. To handle the long-tailed distribution of training data and encourage the learning of long sequence tokens, we use progressively-balanced sampling [14]. This strategy interpolates between instance-balanced sampling and class-balanced sampling during training. For class j , which we classify per 100 faces, the sampling probability $p_j^{PB}(t)$ at epoch t is:

$$p_j^{PB}(t) = (1 - t/T)p_j^{IB} + (t/T)p_j^{CB}$$

where p_j^{IB} and p_j^{CB} are the probabilities for instance-balanced and class-balanced sampling, t is the current epoch, and T is the total number of epochs. Early epochs focus on instance-balanced sampling ($t \rightarrow 0$), while later epochs prioritize class-balanced sampling ($t \rightarrow T$), enabling effective learning of long-tailed classes with long token sequence..

Loss Function. To train the auto-regressive model, we utilize the standard cross-entropy loss function, which minimizes the difference between the predicted token logits and the ground truth token sequence. The loss is expressed as:

$$\mathcal{L}_{ce} = - \sum_{t=1}^{T-1} S_{t+1} \log \hat{S}_t$$

where \hat{S}_t refers to the predicted logits at time step t , and S_{t+1} denotes the corresponding one-hot encoded ground truth token at the next time step.

4 Experiments

4.1 Dataset and Metrics

Datasets. The model is trained on the mixture of gObjaverse [50; 23] (a subset of Objaverse [8] with ~280k meshes), ShapeNetV2 [1], 3D-FUTURE [9] and Toys4K [30] with around 100K meshes without manual selection. The meshes with token length > 10000 and max vertex number per layer $> m$ ($m=200$) are filtered. Following TreeMeshGPT [19], 1000 meshes of gObjaverse and 200 meshes of other datasets are sampled and reserved for evaluation, with the remainder used for training.

Metrics. We apply four metrics to evaluate the point cloud conditioned generation quality, including Chamfer Distance (CD), Hausdorff Distance (HD), Normal Consistency (NC and INCI). CD and HD are geometric metrics used to evaluate the similarity between point clouds or meshes. Normal Consistency (NC) assesses the alignment of surface normals, with higher values indicating better consistency. Its absolute form, INCI, removes directional polarity, focusing purely on overall normal consistency. In addition, we defined a new metric FR named face number ratio to evaluate the new face generation ability of auto-regressive model, which is calculated by: $FR = f_{pred}/f_{gt}$, where f_{pred} is the number of faces of generated mesh and f_{gt} is the face number of ground truth mesh.

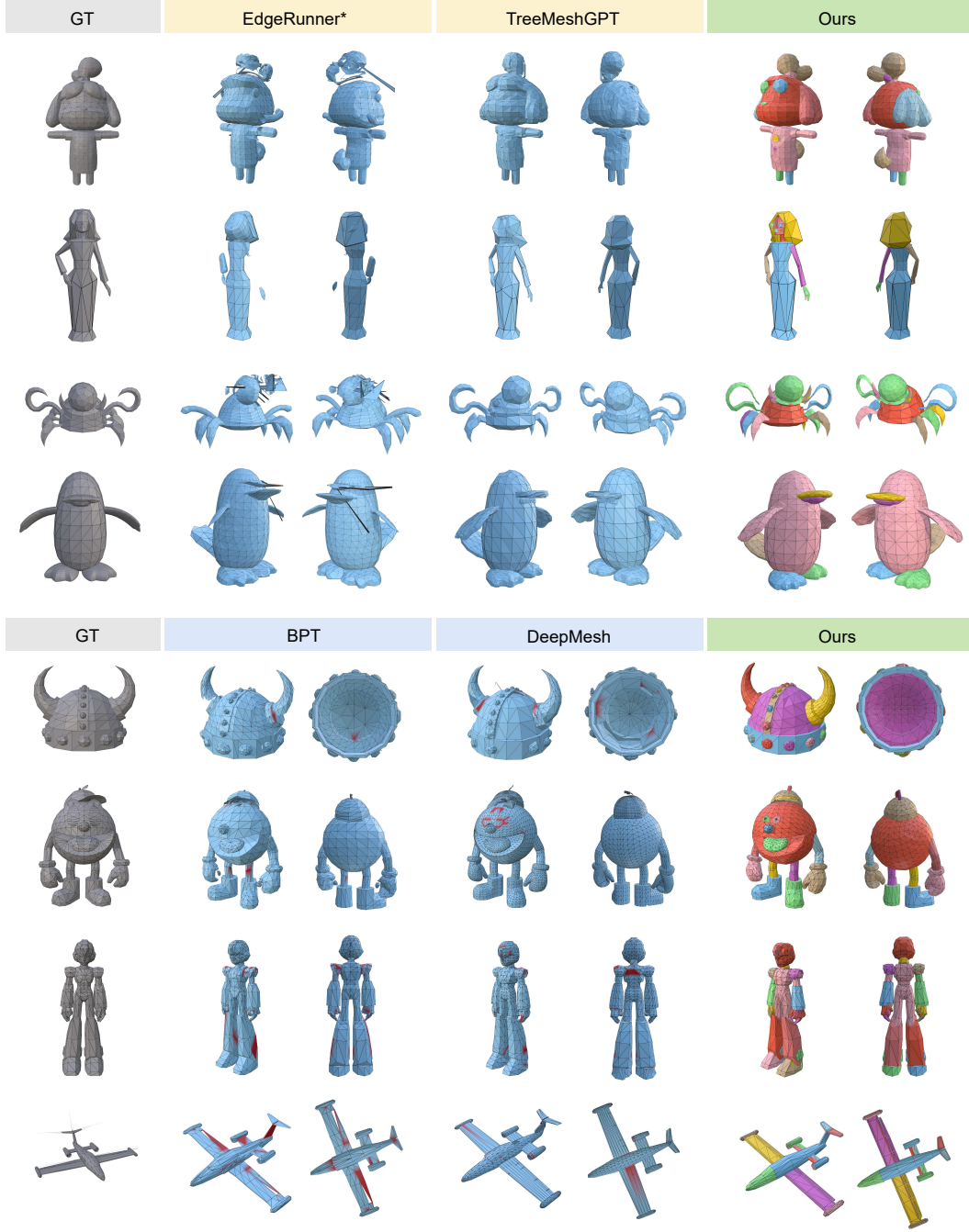


Figure 6: Qualitative Comparison on EdgeRunner* [31], TreeMeshGPT [19], BPT [38], DeepMesh [47], and our method. The * denotes faithful training on the same dataset as ours. The connected components of our generated meshes are colored since our model is connected component aware based on token **C** and can capture details for minute connected components. (1). For tree-traversal methods EdgeRunner and TreeMeshGPT, the manifold topology for generated mesh is guaranteed, while our method demonstrates more robust generation capability and generates more details. (2). We achieved comparable visual results Compared to local patch methods BPT and DeepMesh. However, these methods can not generate meshes with manifold topology, which hinders practical application. The non-manifold edges are colored with **red** for BPT and DeepMesh.

Table 1: Quantitative comparison on baselines. Our method offers higher geometric accuracy and tends to generate more faces than ground truth as shown in FR. The * denotes faithful training on the same dataset as ours. See Appendix D for analysis about compression ratio.

| Method | CD ↓ | HD ↓ | NC ↑ | INCl ↑ | FR ↑ | Comp. Ratio ↓ |
|------------------|--------------|--------------|--------------|--------------|--------------|---------------|
| EdgeRunner* [31] | 0.140 | 0.296 | 0.322 | 0.586 | 1.222 | 0.47 |
| TreeMeshGPT [19] | 0.083 | 0.165 | 0.483 | 0.629 | 1.300 | 0.22 |
| BPT [38] | 0.080 | 0.147 | 0.682 | 0.793 | 0.780 | 0.26 |
| Ours | 0.079 | 0.142 | 0.708 | 0.830 | 1.321 | 0.22 |

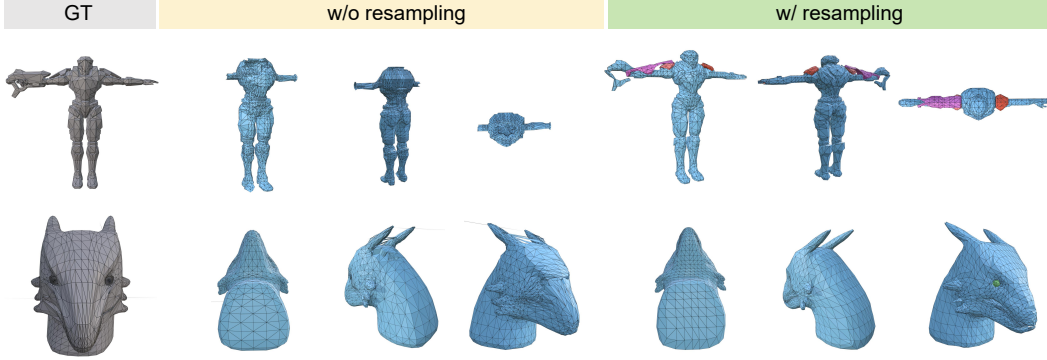


Figure 7: Ablation study on the resampling strategy. The visualization shows that our model achieves a more robust mesh generation capability with the resampling strategy than with the naive sampling.

4.2 Implementation Details

The decoder-only transformer has 24 layers and a hidden size of 1024, and the trainable parameter number is around 500M. It is trained on $16 \times \text{H800}$ with around 15 days. The AdamW [21] is used as optimizer with $\beta_1=0.9$, $\beta_2=0.99$ and the learning rate starts from $1e^{-4}$ and decreases to $5e^{-5}$ based on cosine curve. More details are presented in the Appendix.

4.3 Comparison Results

Quantitative Results. To benchmark the capability of mesh generation for our method, we use 500 meshes randomly sampled from reserved gObjaverse [50; 23] dataset for evaluation. We select EdgeRunner [31], TreeMeshGPT [19], BPT [38] as the baselines. For EdgeRunner, we trained the model on the same dataset as ours (the meshes with face number $> 4k$ are filtered) and followed the released training setting since only the training script is released. The five metrics: CD, HD, NC, INCl, FR, and total compression ratio are presented in Tab. 1. Our method demonstrates better geometric quality and can generate meshes with higher face numbers as shown by FR.

Qualitative Results. We compare the qualitative results with EdgeRunner [31], TreeMeshGPT [19], BPT [38] and DeepMesh [47]. As shown in Fig. 6, our method shows robust generation capability, more mesh details, and strict manifold topology. We list our advantages in the figure caption.

4.4 Ablation Study

Table 2: Ablation study on the resampling strategy.

| Strategy | CD ↓ | HD ↓ | NC ↑ | INCl ↑ | FR ↑ |
|----------------|--------------|--------------|--------------|--------------|--------------|
| w/o resampling | 0.095 | 0.182 | 0.643 | 0.788 | 1.266 |
| w resampling | 0.079 | 0.142 | 0.708 | 0.830 | 1.321 |

The progressively-balanced sampling [14] plays an important role in generation quality since the training data displays a long-tailed distribution without manual selection. For training data, we assign object categories at intervals of every 100 faces, resulting in a distinct long-tail distribution: the categories with fewer faces are concentrated in the head, while categories with larger face counts

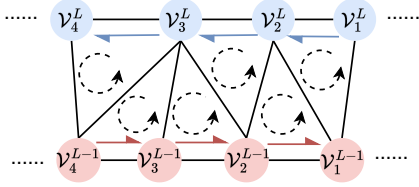


Figure 8: Illustration of face normal consistency. Half-edges of layer L are pointing from lower order to higher order, while the layer $L - 1$ is opposite.

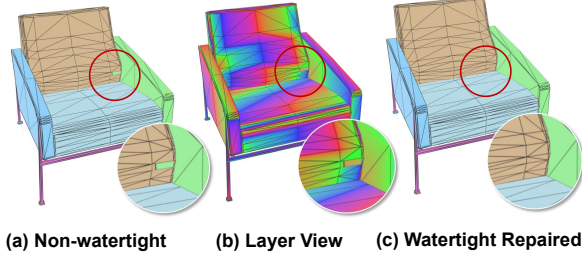


Figure 9: Example of watertight detection and repair. The red-green-blue vertices in (b) denote the layer $3L$, $3L + 1$, $3L + 2$ respectively, where the missing faces is easily to be detected and repaired.

dominate the tail. Without the resampling strategy, the model is prone to overfitting on simpler object categories, leading to a bias toward generating meshes with fewer faces, as illustrated in Fig. 7.

To address this, the progressive-balanced sampling strategy is employed. During the early stages, instance-balanced resampling is utilized for the model, capturing the characteristics of different samples. In later stages, class-balanced resampling is applied, ensuring equitable learning across various objects with different faces. This progressive strategy enhances the model’s ability to generate meshes with diverse and complex topological structures, as illustrated in Tab. 2 and Fig. 7.

4.5 Geometric Properties

Face Normal Consistency. When decoding triangles from predicted token sequences, the triangles decoded by our method satisfy strong normal orientation constraints, ensuring that no flipped triangles are decoded. This advantageous property is well reflected in the NC and INCI metrics in Tab. 1. To explain this, we take Fig. 8 as an example. Once the vertex positions of layer L and $L - 1$, as well as the between-layer matrix have been obtained, the triangles between layers will always have at least two vertices belonging to the same layer. For layer L , we define the direction of the half-edge as ascending along the vertex order, while for layer $L - 1$, the operation is reversed, as shown in the blue and red arrow in Fig. 8. This simple constraint ensures that all triangle vertices are traversed in a counterclockwise order. When calculating the face normals, the cross-product is calculated based on half-edge vectors, resulting in consistent normal orientations.

Watertight Detection and Repair. Considering the instability inherent in autoregressive models, topology token prediction errors may occasionally occur, leading to holes in mesh surfaces that are expected to be watertight. This phenomenon is also commonly observed in other autoregressive mesh generation methods. However, our mesh representation inherently supports watertight detection and repair in a certain degree. This post-processing step effectively mitigates the impact of autoregressive model’s instability, offering an advantage that other mesh tokenization methods lack. As shown in Fig. 9 (b), we visualize each layer of vertices with red-green-blue contour line. It is obvious that surface holes are invariably caused by certain entries in the self-layer matrix or between-layer matrix being incorrectly predicted as 0 instead of 1. Based on the connection rules in Sec. 3.3, such anomalies can be easily detected by our algorithm. The same principle applies to the self-layer matrix.

5 Conclusion

In summary, we propose a compact and efficient mesh tokenization algorithm that achieves further compression than peer methods by encoding each vertex only once, reducing the compression ratio from 0.26 to 0.22 and minimizing redundant information of sequence. The advantages of this algorithm lie in its ability to generate as many triangles as possible under limited token length. It also focuses on small yet critical geometric connected components during the mesh generation. Moreover, our algorithm exhibits excellent topological properties, which are crucial for downstream applications, such as manifold topology, watertight detection support, and consistent face normals.

Limitation. One limitation of our method lies in the increased vocabulary size. In addition to tokens representing vertices, our approach also includes tokens for self-layer and between-layer matrices, resulting in a final vocabulary size up to 10,267. Furthermore, our method requires the predefinition

of the maximum supported matrix size m , which corresponds to the maximum number of vertices per layer. This constraint necessitates filtering the dataset according to this rule, potentially excluding certain types of data and thereby affecting generalization. Moreover, we believe that the full potential of our method remains underexplored. For instance, extending its support to quadrilateral or hybrid polygon compression represents a promising direction for future research.

References

- [1] Angel X Chang, Thomas Funkhouser, Leonidas Guibas, Pat Hanrahan, Qixing Huang, Zimo Li, Silvio Savarese, Manolis Savva, Shuran Song, Hao Su, et al. Shapenet: An information-rich 3d model repository. *arXiv preprint arXiv:1512.03012*, 2015.
- [2] Sijin Chen, Xin Chen, Anqi Pang, Xianfang Zeng, Wei Cheng, Yijun Fu, Fukun Yin, Billzb Wang, Jingyi Yu, Gang Yu, et al. Meshxl: Neural coordinate field for generative 3d foundation models. *Advances in Neural Information Processing Systems*, 37:97141–97166, 2024.
- [3] Yiwen Chen, Tong He, Di Huang, Weicai Ye, Sijin Chen, Jiaxiang Tang, Xin Chen, Zhongang Cai, Lei Yang, Gang Yu, et al. Meshanything: Artist-created mesh generation with autoregressive transformers. *arXiv preprint arXiv:2406.10163*, 2024.
- [4] Yiwen Chen, Yikai Wang, Yihao Luo, Zhengyi Wang, Zilong Chen, Jun Zhu, Chi Zhang, and Guosheng Lin. Meshanything v2: Artist-created mesh generation with adjacent mesh tokenization. *arXiv preprint arXiv:2408.02555*, 2024.
- [5] Zhaoxi Chen, Jiaxiang Tang, Yuhao Dong, Ziang Cao, Fangzhou Hong, Yushi Lan, Tengfei Wang, Haozhe Xie, Tong Wu, Shunsuke Saito, et al. 3dtopia-xl: Scaling high-quality 3d asset generation via primitive diffusion. *arXiv preprint arXiv:2409.12957*, 2024.
- [6] Zilong Chen, Feng Wang, Yikai Wang, and Huaping Liu. Text-to-3d using gaussian splatting. In *Proceedings of the IEEE/CVF conference on computer vision and pattern recognition*, pages 21401–21412, 2024.
- [7] Matt Deitke, Ruoshi Liu, Matthew Wallingford, Huong Ngo, Oscar Michel, Aditya Kusupati, Alan Fan, Christian Laforte, Vikram Voleti, Samir Yitzhak Gadre, et al. Objaverse-xl: A universe of 10m+ 3d objects. *Advances in Neural Information Processing Systems*, 36:35799–35813, 2023.
- [8] Matt Deitke, Dustin Schwenk, Jordi Salvador, Luca Weihs, Oscar Michel, Eli VanderBilt, Ludwig Schmidt, Kiana Ehsani, Aniruddha Kembhavi, and Ali Farhadi. Objaverse: A universe of annotated 3d objects. *arXiv preprint arXiv:2212.08051*, 2022.
- [9] Huan Fu, Rongfei Jia, Lin Gao, Mingming Gong, Binqiang Zhao, Steve Maybank, and Dacheng Tao. 3d-future: 3d furniture shape with texture. *International Journal of Computer Vision*, 129:3313–3337, 2021.
- [10] PL George and H Borouchaki. Delaunay triangulation and meshing: Application to finite elements. 1998. *Hermes, Paris*.
- [11] Zekun Hao, David W Romero, Tsung-Yi Lin, and Ming-Yu Liu. Meshtron: High-fidelity, artist-like 3d mesh generation at scale. *arXiv preprint arXiv:2412.09548*, 2024.
- [12] Yicong Hong, Kai Zhang, Jiuxiang Gu, Sai Bi, Yang Zhou, Difan Liu, Feng Liu, Kalyan Sunkavalli, Trung Bui, and Hao Tan. Lrm: Large reconstruction model for single image to 3d. *arXiv preprint arXiv:2311.04400*, 2023.
- [13] Zixuan Huang, Mark Boss, Aaryaman Vasishta, James M Rehg, and Varun Jampani. Spar3d: Stable point-aware reconstruction of 3d objects from single images. *arXiv preprint arXiv:2501.04689*, 2025.
- [14] Bingyi Kang, Saining Xie, Marcus Rohrbach, Zhicheng Yan, Albert Gordo, Jiashi Feng, and Yannis Kalantidis. Decoupling representation and classifier for long-tailed recognition. *arXiv preprint arXiv:1910.09217*, 2019.

- [15] Jiahao Li, Hao Tan, Kai Zhang, Zexiang Xu, Fujun Luan, Yinghao Xu, Yicong Hong, Kalyan Sunkavalli, Greg Shakhnarovich, and Sai Bi. Instant3d: Fast text-to-3d with sparse-view generation and large reconstruction model. *arXiv preprint arXiv:2311.06214*, 2023.
- [16] Weiyu Li, Rui Chen, Xuelin Chen, and Ping Tan. Sweetdreamer: Aligning geometric priors in 2d diffusion for consistent text-to-3d. *arXiv preprint arXiv:2310.02596*, 2023.
- [17] Weiyu Li, Jiarui Liu, Rui Chen, Yixun Liang, Xuelin Chen, Ping Tan, and Xiaoxiao Long. Craftsman: High-fidelity mesh generation with 3d native generation and interactive geometry refiner. *arXiv preprint arXiv:2405.14979*, 2024.
- [18] Chen-Hsuan Lin, Jun Gao, Luming Tang, Towaki Takikawa, Xiaohui Zeng, Xun Huang, Karsten Kreis, Sanja Fidler, Ming-Yu Liu, and Tsung-Yi Lin. Magic3d: High-resolution text-to-3d content creation. In *Proceedings of the IEEE/CVF conference on computer vision and pattern recognition*, pages 300–309, 2023.
- [19] Stefan Lionar, Jiabin Liang, and Gim Hee Lee. Treemeshgpt: Artistic mesh generation with autoregressive tree sequencing. *arXiv preprint arXiv:2503.11629*, 2025.
- [20] William E Lorensen and Harvey E Cline. Marching cubes: A high resolution 3d surface construction algorithm. In *Seminal graphics: pioneering efforts that shaped the field*, pages 347–353. 1998.
- [21] Ilya Loshchilov and Frank Hutter. Decoupled weight decay regularization. *arXiv preprint arXiv:1711.05101*, 2017.
- [22] Piotr Nawrot, Szymon Tworkowski, Michał Tyrolski, Łukasz Kaiser, Yuhuai Wu, Christian Szegedy, and Henryk Michalewski. Hierarchical transformers are more efficient language models. *arXiv preprint arXiv:2110.13711*, 2021.
- [23] Lingteng Qiu, Guanying Chen, Xiaodong Gu, Qi Zuo, Mutian Xu, Yushuang Wu, Weihao Yuan, Zilong Dong, Liefeng Bo, and Xiaoguang Han. Richdreamer: A generalizable normal-depth diffusion model for detail richness in text-to-3d. In *Proceedings of the IEEE/CVF Conference on Computer Vision and Pattern Recognition*, pages 9914–9925, 2024.
- [24] Rafael Rafailov, Archit Sharma, Eric Mitchell, Christopher D Manning, Stefano Ermon, and Chelsea Finn. Direct preference optimization: Your language model is secretly a reward model. *Advances in Neural Information Processing Systems*, 36:53728–53741, 2023.
- [25] Amit Raj, Srinivas Kaza, Ben Poole, Michael Niemeyer, Nataniel Ruiz, Ben Mildenhall, Shiran Zada, Kfir Aberman, Michael Rubinstein, Jonathan Barron, et al. Dreambooth3d: Subject-driven text-to-3d generation. In *Proceedings of the IEEE/CVF international conference on computer vision*, pages 2349–2359, 2023.
- [26] Robin Rombach, Andreas Blattmann, Dominik Lorenz, Patrick Esser, and Björn Ommer. High-resolution image synthesis with latent diffusion models. In *Proceedings of the IEEE/CVF conference on computer vision and pattern recognition*, pages 10684–10695, 2022.
- [27] Jonathan Richard Shewchuk. Delaunay refinement algorithms for triangular mesh generation. *Computational geometry*, 22(1-3):21–74, 2002.
- [28] Yichun Shi, Peng Wang, Jianglong Ye, Mai Long, Kejie Li, and Xiao Yang. Mvdream: Multi-view diffusion for 3d generation. *arXiv preprint arXiv:2308.16512*, 2023.
- [29] Yawar Siddiqui, Antonio Alliegro, Alexey Artemov, Tatiana Tommasi, Daniele Sirigatti, Vladislav Rosov, Angela Dai, and Matthias Nießner. Meshgpt: Generating triangle meshes with decoder-only transformers. In *Proceedings of the IEEE/CVF conference on computer vision and pattern recognition*, pages 19615–19625, 2024.
- [30] Stefan Stojanov, Anh Thai, and James M Rehg. Using shape to categorize: Low-shot learning with an explicit shape bias. In *Proceedings of the IEEE/CVF conference on computer vision and pattern recognition*, pages 1798–1808, 2021.

- [31] Jiaxiang Tang, Zhaoshuo Li, Zekun Hao, Xian Liu, Gang Zeng, Ming-Yu Liu, and Qinsheng Zhang. Edgerunner: Auto-regressive auto-encoder for artistic mesh generation. *arXiv preprint arXiv:2409.18114*, 2024.
- [32] Jiaxiang Tang, Jiawei Ren, Hang Zhou, Ziwei Liu, and Gang Zeng. Dreamgaussian: Generative gaussian splatting for efficient 3d content creation. *arXiv preprint arXiv:2309.16653*, 2023.
- [33] William Thomas Tutte. A census of planar maps. *Canadian Journal of Mathematics*, 15:249–271, 1963.
- [34] Aaron Van Den Oord, Oriol Vinyals, et al. Neural discrete representation learning. *Advances in neural information processing systems*, 30, 2017.
- [35] Tengfei Wang, Bo Zhang, Ting Zhang, Shuyang Gu, Jianmin Bao, Tadas Baltrusaitis, Jingjing Shen, Dong Chen, Fang Wen, Qifeng Chen, et al. Rodin: A generative model for sculpting 3d digital avatars using diffusion. In *Proceedings of the IEEE/CVF conference on computer vision and pattern recognition*, pages 4563–4573, 2023.
- [36] Yuxuan Wang, Xuanyu Yi, Haohan Weng, Qingshan Xu, Xiaokang Wei, Xianghui Yang, Chunchao Guo, Long Chen, and Hanwang Zhang. Nautilus: Locality-aware autoencoder for scalable mesh generation. *arXiv preprint arXiv:2501.14317*, 2025.
- [37] Zhengyi Wang, Jonathan Lorraine, Yikai Wang, Hang Su, Jun Zhu, Sanja Fidler, and Xiaohui Zeng. Llama-mesh: Unifying 3d mesh generation with language models. *arXiv preprint arXiv:2411.09595*, 2024.
- [38] Haohan Weng, Zibo Zhao, Biwen Lei, Xianghui Yang, Jian Liu, Zeqiang Lai, Zhuo Chen, Yuhong Liu, Jie Jiang, Chunchao Guo, et al. Scaling mesh generation via compressive tokenization. *arXiv preprint arXiv:2411.07025*, 2024.
- [39] Shuang Wu, Youtian Lin, Feihu Zhang, Yifei Zeng, Jingxi Xu, Philip Torr, Xun Cao, and Yao Yao. Direct3d: Scalable image-to-3d generation via 3d latent diffusion transformer. *arXiv preprint arXiv:2405.14832*, 2024.
- [40] Jianfeng Xiang, Zelong Lv, Sicheng Xu, Yu Deng, Ruicheng Wang, Bowen Zhang, Dong Chen, Xin Tong, and Jiaolong Yang. Structured 3d latents for scalable and versatile 3d generation. *arXiv preprint arXiv:2412.01506*, 2024.
- [41] Jiale Xu, Weihao Cheng, Yiming Gao, Xintao Wang, Shenghua Gao, and Ying Shan. Instantmesh: Efficient 3d mesh generation from a single image with sparse-view large reconstruction models. *arXiv preprint arXiv:2404.07191*, 2024.
- [42] Xianghui Yang, Huiwen Shi, Bowen Zhang, Fan Yang, Jiacheng Wang, Hongxu Zhao, Xinhai Liu, Xinzhou Wang, Qingxiang Lin, Jiaao Yu, et al. Hunyuan3d 1.0: A unified framework for text-to-3d and image-to-3d generation. *arXiv preprint arXiv:2411.02293*, 2024.
- [43] Junliang Ye, Fangfu Liu, Qixiu Li, Zhengyi Wang, Yikai Wang, Xinzhou Wang, Yueqi Duan, and Jun Zhu. Dreamreward: Text-to-3d generation with human preference. In *European Conference on Computer Vision*, pages 259–276. Springer, 2024.
- [44] Taoran Yi, Jiemin Fang, Junjie Wang, Guanjun Wu, Lingxi Xie, Xiaopeng Zhang, Wenyu Liu, Qi Tian, and Xinggang Wang. Gaussiandreamer: Fast generation from text to 3d gaussians by bridging 2d and 3d diffusion models. In *Proceedings of the IEEE/CVF Conference on Computer Vision and Pattern Recognition*, pages 6796–6807, 2024.
- [45] Biao Zhang, Jiapeng Tang, Matthias Niessner, and Peter Wonka. 3dshape2vecset: A 3d shape representation for neural fields and generative diffusion models. *ACM Transactions On Graphics (TOG)*, 42(4):1–16, 2023.
- [46] Longwen Zhang, Ziyu Wang, Qixuan Zhang, Qiwei Qiu, Anqi Pang, Haoran Jiang, Wei Yang, Lan Xu, and Jingyi Yu. Clay: A controllable large-scale generative model for creating high-quality 3d assets. *ACM Transactions on Graphics (TOG)*, 43(4):1–20, 2024.

- [47] Ruowen Zhao, Junliang Ye, Zhengyi Wang, Guangce Liu, Yiwen Chen, Yikai Wang, and Jun Zhu. Deepmesh: Auto-regressive artist-mesh creation with reinforcement learning. *arXiv preprint arXiv:2503.15265*, 2025.
- [48] Zibo Zhao, Zeqiang Lai, Qingxiang Lin, Yunfei Zhao, Haolin Liu, Shuhui Yang, Yifei Feng, Mingxin Yang, Sheng Zhang, Xianghui Yang, et al. Hunyuan3d 2.0: Scaling diffusion models for high resolution textured 3d assets generation. *arXiv preprint arXiv:2501.12202*, 2025.
- [49] Zibo Zhao, Wen Liu, Xin Chen, Xianfang Zeng, Rui Wang, Pei Cheng, Bin Fu, Tao Chen, Gang Yu, and Shenghua Gao. Michelangelo: Conditional 3d shape generation based on shape-image-text aligned latent representation. *Advances in neural information processing systems*, 36:73969–73982, 2023.
- [50] Qi Zuo, Xiaodong Gu, Yuan Dong, Zhengyi Zhao, Weihao Yuan, Lingteng Qiu, Liefeng Bo, and Zilong Dong. High-fidelity 3d textured shapes generation by sparse encoding and adversarial decoding. In *European Conference on Computer Vision*, 2024.

Appendix

Introduction of Appendix

The appendix has six sections to introduce more details of our method, implementation details and experimental results.

- Sec. **A** introduces more complex scenarios of **non-manifold processing** in Sec. 3.1 of main paper body.
- Sec. **B** introduces some special case of **self-layer matrix compression** in Sec. 3.3 of main paper body.
- Sec. **C** introduces the full version of **between-layer matrix compression** in Sec. 3.3 of main paper body.
- Sec. **D** shows the analysis and derivation of our **compression ratio** in Table 1 of main paper body.
- Sec. **E** shows more results of our **text-conditioned** mesh generation and **image-conditioned** mesh generation.
- Sec. **F** introduces more **implementation details** of our experiments.

A Non-manifold Processing

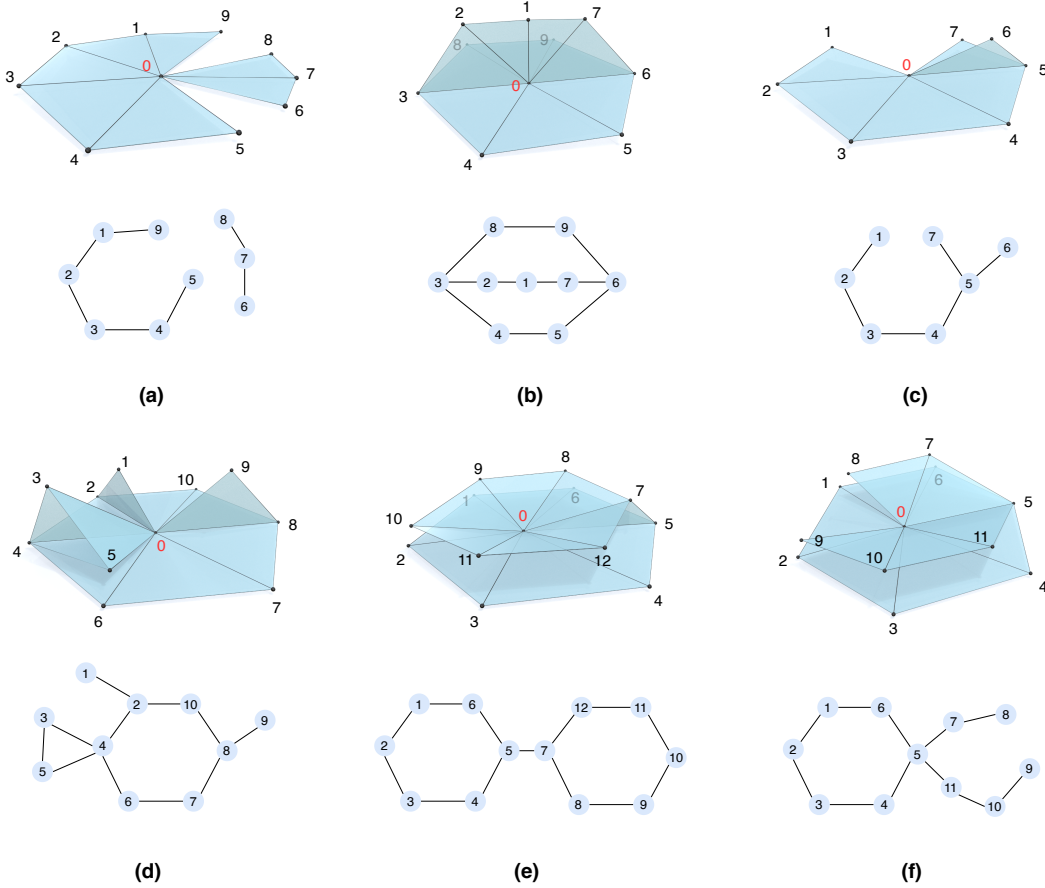


Figure 10: Illustration of six non-manifold scenarios. The non-manifold vertex 0 is marked as red, and all of each scenario is equal to an equivalent edge graph \mathcal{G}_0 under the mesh.

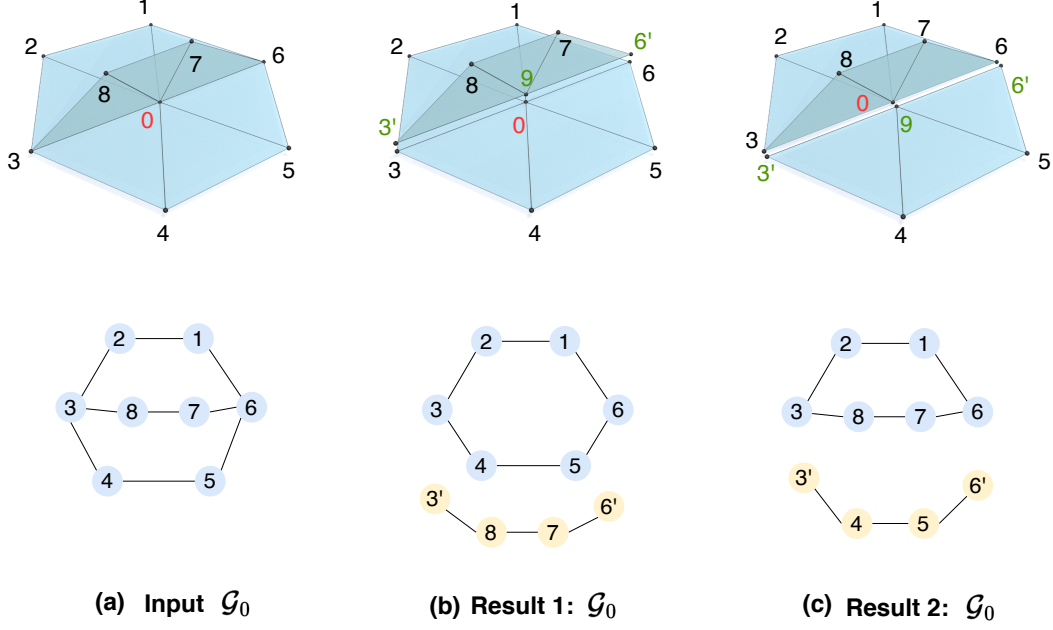


Figure 11: Illustration of Rule 1: Max Cycle or Max Chain First. Given input \mathcal{G}_0 , we list two different partition results, and either of the result is reasonable temporarily. The vertex "9" indicates the new generated vertex due to edge graph partition, with same coordinate of vertex "0".

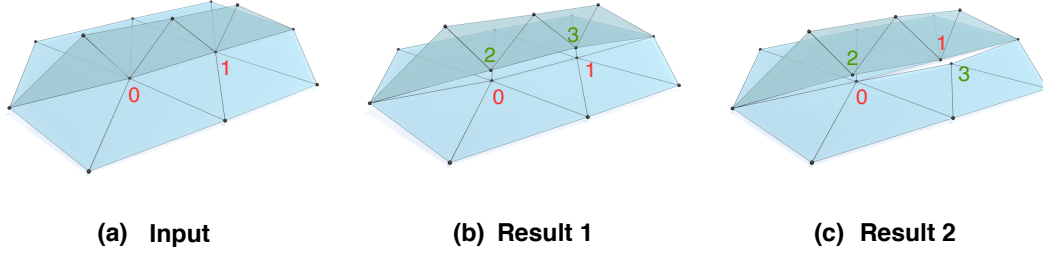


Figure 12: Illustration of the success case and failure case of Rule 1. The vertices "0", "1" are processed based on Rule 1, with "2", "3" are new generated vertices from edge graph partition. This will lead to two different results: (b) is success case since the completeness of surface is kept, while (c) is the failure case with broken surface.

In this section, we introduce our non-manifold processing algorithm for more complex scenarios. First, we present additional examples of non-manifold vertices along with their corresponding edge graph representations. To address these complex situations, we propose three key rules for the edge graph partitioning algorithm to ensure the integrity of the local surface: (1) Max cycle or max chain first. (2) Mesh connected component first. (3) Breadth-First-Search (BFS) processing. The rationale behind these rules is explained in details in the following subsections.

A.1 Equivalent Transform from Mesh to Edge Graph

As illustrated in Fig. 10, we present six different scenarios, encompassing both simple and complex examples. Scenario (a) represents the simplest case. In the equivalent edge graph, there are two connected components that can be directly partitioned. Scenario (b) is another common case, featuring three sub-cycles in the edge graph. Scenario (c) is a boundary case, as there are no cycles present. Scenarios (d)(e)(f) demonstrate more complex cases, involving several different cycles or chains.

A.2 Partition Rule 1: Max Cycle or Max Chain First

In our algorithm, scenario like (a) in Fig. 10 is handled first to ensure that each edge graph contains only one connected component. Next, cycles or chains are detected, and the cycle with the maximum length is selected and retained, while the remaining edges are detached. For example, in scenario like Fig. 10 (d), the cycle 2-4-6-7-8-10-2 is retained, and the other edges will be detached. If no cycle exists, the chain with the maximum length is selected.

If there are two or more cycles of equal length in the edge graph, any of these cycles may be selected, and all such choices are considered reasonable. As illustrated in Fig. 11, the input \mathcal{G}_0 contains three sub-cycles: 1-2-3-4-5-6-1, 1-2-3-8-7-6-1, and 3-4-5-6-7-8-3. We provide two different partition results, both of which are temporarily acceptable for our algorithm.

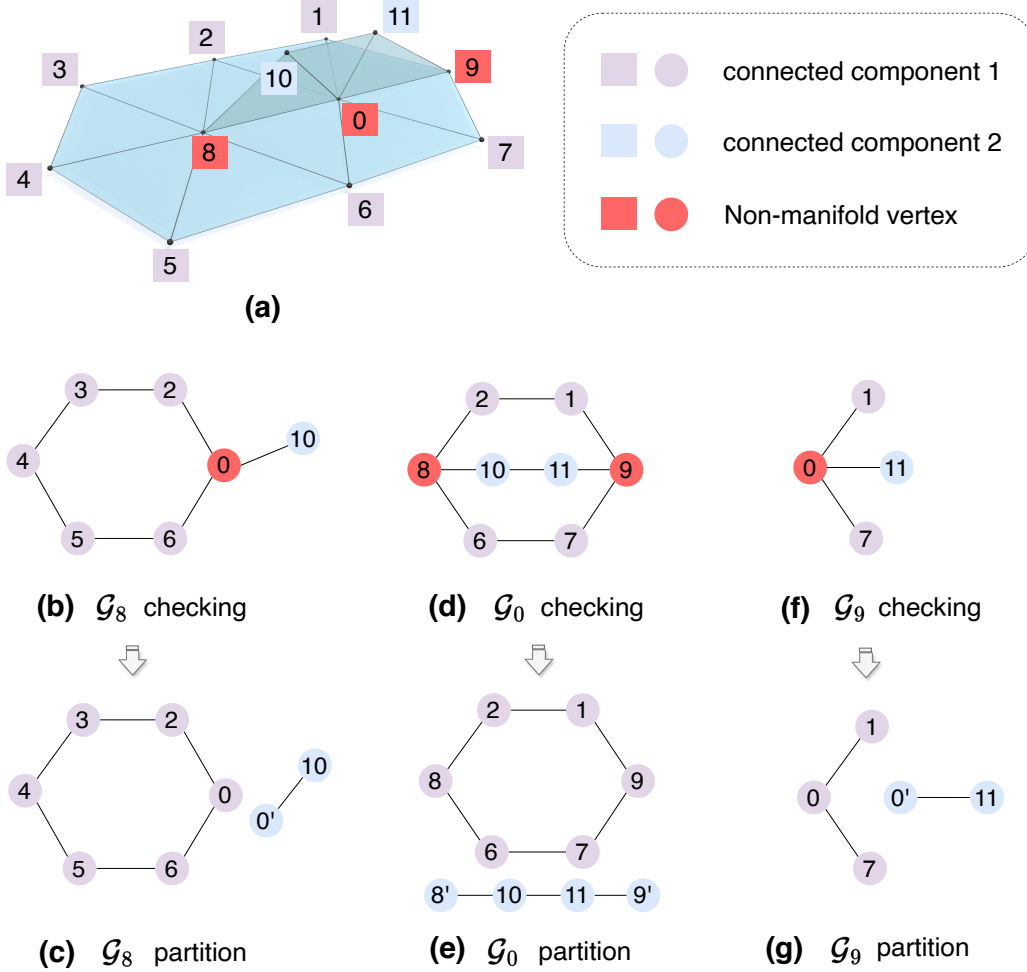


Figure 13: Illustration of Rule 2: Mesh Connected Component First. In the edge graph, the vertices belong to the same mesh connected component should be partitioned together as much as possible to keep the integrity of the whole mesh.

A.3 Partition Rule 2: Mesh Connected Component First

For a specific edge graph, Rule 1 may appear sufficient; however, when considering two connected non-manifold vertices, the completeness of the local surface is not guaranteed. As illustrated in Fig. 12, applying the simple "max cycle or max chain first" rule can lead to two different partition results, as shown in (b) and (c). While (b) preserves surface integrity, (c) represents a failure case, as the surface integrity has been compromised. Therefore, the edge graph partitioning process should not only focus on a specific vertex but also consider its connected vertices.

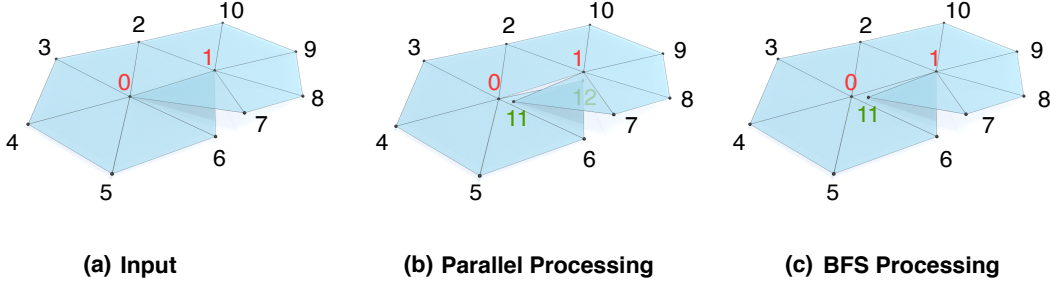


Figure 14: Illustration of parallel processing and Rule 3: BFS processing. Since the edge graph partition algorithm can affect surrounding vertices and potentially convert non-manifold vertices into manifold vertices, using the BFS algorithm to process them sequentially will result in less surface fragmentation.

To address this issue, we first assign a mesh connected component index (distinct from the connected components of the edge graph) to each manifold vertex, while marking non-manifold vertices with a special mesh connected component index. As illustrated in Fig. 13 (a), all connected manifold vertices share the same mesh connected component index, where vertices $\{1,2,3,4,5,6,7\}$ and $\{10,11\}$ are grouped together, respectively.

Secondly, when checking the edge graph, vertices belonging to the same mesh connected component should be grouped together as much as possible, and this rule should take precedence over Rule 1. For example, in Fig. 13 (d) and (e), when checking \mathcal{G}_0 , three sub-cycles are available. However, the cycle 1-2-8-6-7-9-1 must be selected because vertices 1,2,6,7 belong to the same mesh connected component.

In the edge graph, non manifold vertices are marked as special mesh connected components (red color in Fig. 13) and should ultimately be assigned to the mesh connected component of a manifold vertex. Therefore, the partition rule 2 should prioritize connecting edge graph vertices that belong to the same mesh connected component as much as possible.

A.4 Partition Rule 3: BFS Processing

After establishing Rule 1 and Rule 2, an unresolved issue remains: whether non-manifold vertices should be processed in parallel, specifically through parallel edge graph partitioning, given its higher computational efficiency. However, parallel processing may compromise surface integrity, as demonstrated in Fig. 14. For instance, if non-manifold vertices "0" and "1" are processed in parallel, new vertices "11" and "12" will be generated, and the surfaces near "0" and "1" will become incomplete, as shown in (b).

To address this issue, we propose using the Breadth-First-Search (BFS) algorithm to sequentially process each non-manifold vertex. This sequential approach allows certain adjacent non-manifold vertices to be automatically corrected into manifold vertices, effectively minimizing the generation of redundant vertices and mitigating surface fragmentation. As shown in (c) of Fig. 14, after processing vertex "0", vertex "1" is automatically corrected into a manifold vertex and does not require further processing, while the surface near vertex "0" maintains its integrity.

B Self-Layer Matrix Compression

Generally, if a mesh is topologically homeomorphic to a sphere, the self-layer connections are typically sequential, as shown in Fig. 15 (a)-1. In some occasional cases, several adjacent vertices may form local connections, as shown in Fig. 15 (a)-2. When the topology of the mesh becomes more complex, such as having a genus of 1 (i.e., being homeomorphic to a torus), certain self-layer connections may exhibit configurations as illustrated in Fig. 15 (b)-1, (b)-2.

To compress self-layer matrix, we take Fig. 16 as an example. For sequential connections (a)-2, the matrix is easy to compress and the token number for each row is typically equal to one. In the self-layer matrix (a)-2, the red box denotes compression window with size=3, while the green box

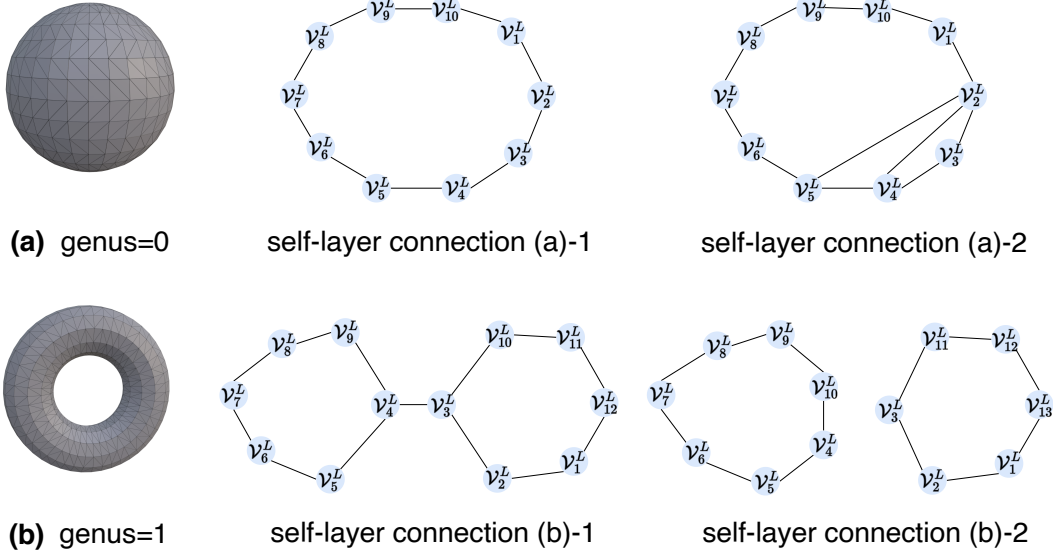


Figure 15: Illustration of several self-layer connections. When the genus=0, the self-layer connections are typically sequential, while the connections become complicated when genus>0.

denotes redundant information and will be set to "0"s in practice. We notice the "1"s typically occur in the compression window since the connections are locally, and the token number for each row remains equal to one.

However, for the self-layer matrix (b)-1, the connections become more complex since several "1"s occur outside compression window. Since the compression window is fixed and does not slide, we use more tokens to compress the row. Take row 3 of self-layer matrix (b)-1 as an example, the "1" in position (3, 10) lies outside the compression window and has an index distance of 3 (starts from 0), we use token index "3" to represent it.

Considering most of the rows still only have one token number, we use a word table with size 2^W , where W is the size of compression window. For rows with more than one token, we use an additional word table with size m to represent extra tokens, where m is the max number of layer vertices, following the same definition of main text.

In practice, we set $W = 8$ and $m = 200$, hence the totally word table size for self-layer matrix is $2^8 + 200 = 456$.

C Between-Layer Matrix Compression

Between-layer connections exhibit different patterns compared to self-layer connections, however, they are interrelated. We illustrate between-layer connections for layer $L + 1$ and L with mesh genus =0 and =1 in Fig. 17. The rules governing the between-layer connections for scenarios (a)-1 and (a)-2 are straightforward, while the rules in scenarios (b)-1 and (b)-2 are more complex.

To efficiently compress between-layer matrix of (a)-1 and (a)-2, we transform the problem into an equivalent "stars and bars" question. Firstly, as shown in Fig. 18, we set a window size $W' = 5$, and place it at the first "1"s of each row, as highlighted by the red boxes. Notice the size of red box is $W' + 1$ since the first element is always "1" and is excluded from consideration in subsequent calculations.

Secondly, after setting the compression window, we denote the finally compressed token index of the window at (i, j) as $F[w_{(i,j)}]$, and transform the representation of "0"s and "1"s in the window to an equivalent "stars and bars" question. We notice in some cases, such as between-layer connections resembling (a)-2 in Fig. 18, the pattern occasionally follows a "1"-0-"1" sequence due to the local self-layer connections in layer L . For example, this is evident in row 2 of the between-layer matrix.

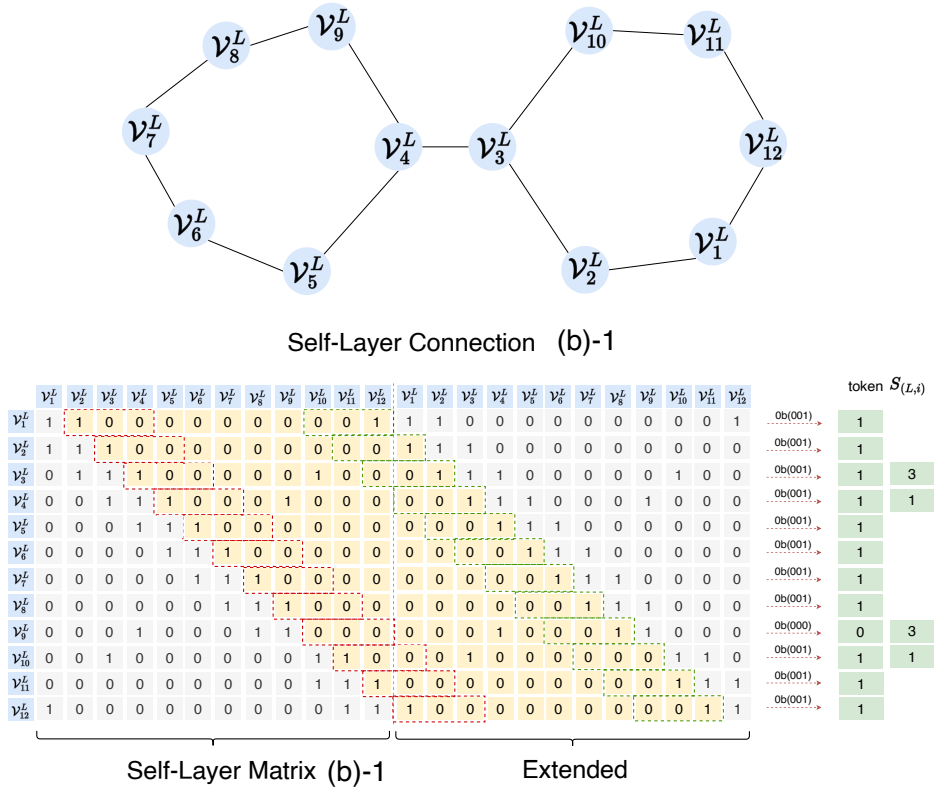
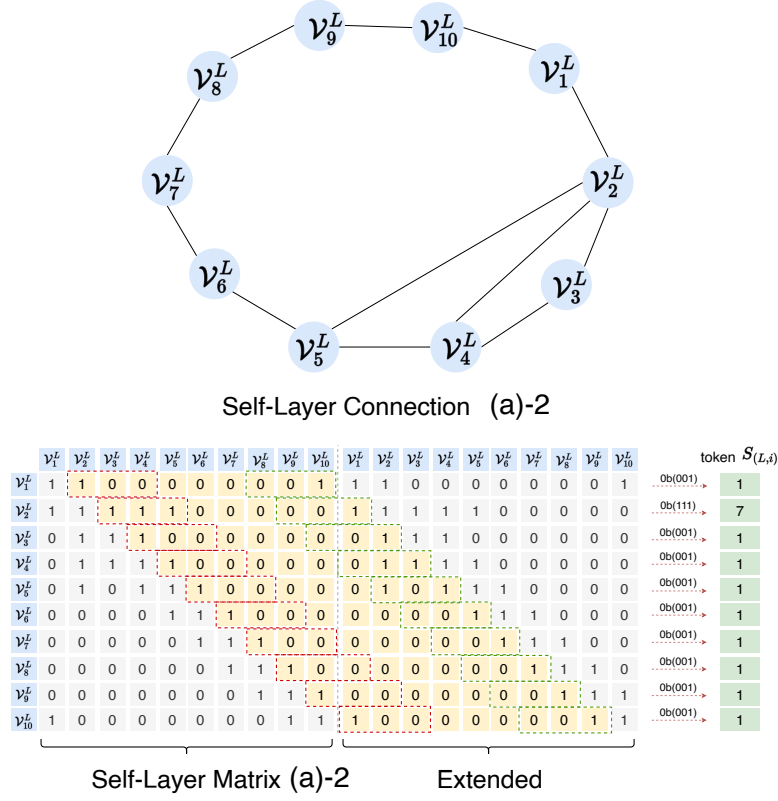
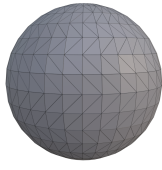
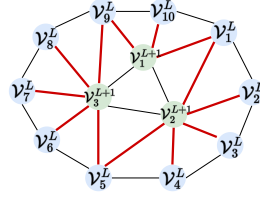


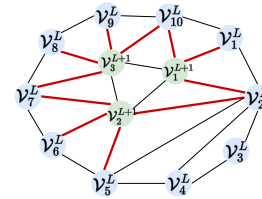
Figure 16: Illustration of self-layer matrix of (a)-2 and (b)-1 in Fig. 15. The red box denotes compression window with size=3, while the green box denotes the redundant information and will be set to "0"s in practice. If "1"s occur outside red box and green box, the token number for the row will be > 1.



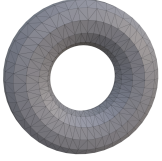
(a) genus=0



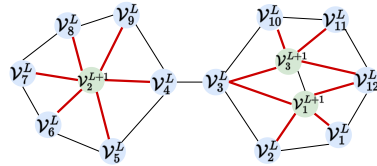
between-layer connection (a)-1



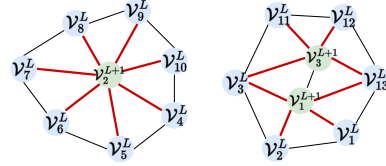
between-layer connection (a)-2



(b) genus=1



between-layer connection (b)-1



between-layer connection (b)-2

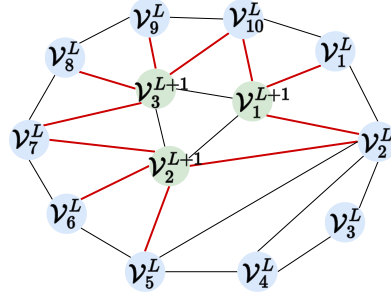
Figure 17: Illustration of between-layer connections for layer $L + 1$ and L . The red lines denote between-layer connections, which are related to self-layer connections of layer L .

To address this, we classify the "stars and bars" question into seven distinct scenarios, as illustrated in Fig. 19.

Finally, the total combinatorial number Y is:

$$Y = 2 \cdot W' + 2 \cdot C_{W'-1}^2 + C_{W'-1}^3$$

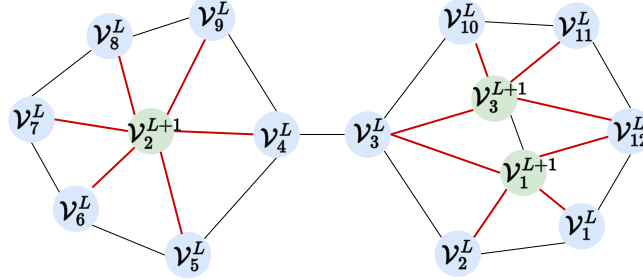
and the total word table size of between-layer matrix is $m \cdot Y$. In practice, we set the $W' = 5$ with $Y=26$, hence the finally word table size of between-layer matrix is 5200.



Between-Layer Connection (a)-2

| | v_1^L | v_2^L | v_3^L | v_4^L | v_5^L | v_6^L | v_7^L | v_8^L | v_9^L | v_{10}^L | | |
|-------------|---------|---------|---------|---------|---------|---------|---------|---------|---------|------------|-----|---|
| v_1^{L+1} | 1 | 1 | 0 | 0 | 0 | 0 | 0 | 0 | 0 | 1 | ... | token $B_{(L+1,i)}$ |
| v_2^{L+1} | 0 | 1 | 0 | 0 | 1 | 1 | 1 | 0 | 0 | 0 | | $1Y + F[w_{(1,1)}]$ $10Y + F[w_{(1,10)}]$ |
| v_3^{L+1} | 0 | 0 | 0 | 0 | 0 | 0 | 1 | 1 | 1 | 1 | ... | $2Y + F[w_{(2,2)}]$ |
| | | | | | | | | | | | | $7Y + F[w_{(3,7)}]$ |

Between-Layer Matrix



Between-Layer Connection (b)-1

| | v_1^L | v_2^L | v_3^L | v_4^L | v_5^L | v_6^L | v_7^L | v_8^L | v_9^L | v_{10}^L | v_{11}^L | v_{12}^L | | |
|-------------|---------|---------|---------|---------|---------|---------|---------|---------|---------|------------|------------|------------|-----|---|
| v_1^{L+1} | 1 | 1 | 1 | 0 | 0 | 0 | 0 | 0 | 0 | 0 | 0 | 1 | ... | token $B_{(L+1,i)}$ |
| v_2^{L+1} | 0 | 0 | 0 | 1 | 1 | 1 | 1 | 1 | 1 | 0 | 0 | 0 | | $1Y + F[w_{(1,1)}]$ $12Y + F[w_{(1,12)}]$ |
| v_3^{L+1} | 0 | 0 | 1 | 0 | 0 | 0 | 0 | 0 | 0 | 1 | 1 | 1 | ... | $4Y + F[w_{(2,4)}]$ |
| | | | | | | | | | | | | | | $3Y + F[w_{(3,3)}]$ $10Y + F[w_{(3,10)}]$ |

Between-Layer Matrix

Figure 18: Illustration of between-layer matrix compression for layer $L + 1$, L . $F[w_{(i,j)}]$ denotes the compressed token index of window (red box) located at (i, j) . We transform the compression of "0"s and "1"s inside the window into an equivalent "stars and bars" question, where Y denotes the totally combinatorial number.

| Scenario | Between layer window | Combinatorial number |
|-----------------|---|----------------------|
| "1" |  | 1 |
| "0" |  | 1 |
| "1"-"0" |  | $C_{W'-1}^1$ |
| "1"-"0"-"1" |  | $C_{W'-1}^2$ |
| "1"-"0"-"1"-"0" |  | $C_{W'-1}^3$ |
| "0"-"1" |  | $C_{W'-1}^1$ |
| "0"-"1"-"0" |  | $C_{W'-1}^2$ |

Figure 19: Illustration of "stars and bars" question for between-layer matrix compression window. We list 7 scenarios, the window size W' is 5.

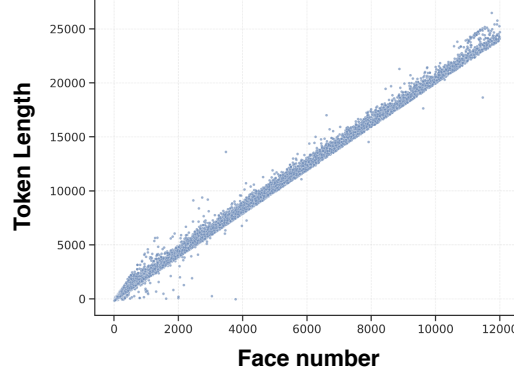


Figure 20: Statistic of the relationship between token length and the number of mesh faces on around 100k data samples. The ratio between them is approximately 2, indicating each face requires two tokens to be encoded on average.

D Compression Ratio Analysis

As illustrated in Fig. 20, we show the statistic result of token length and mesh face number of our dataset with around 100k items. The ratio between token length and face number is approximately equal to 2, meaning it requires 2 tokens to encode one face. Hence the compression ratio should be $2/9 \approx 0.22$.

D.1 Derivation of compression ratio

There is another way to derive the compression ratio $2/9$. Firstly, we suppose the human designed meshes are typically regular triangular meshes with degree equal to 6 on average (see D.2 for derivation). Secondly, we define 3 variables: (1) N_f : the face number of the mesh; (2) N'_v : the vertex number of mesh without deduplication; (3) N_v : the vertex number with deduplication.

It is obvious that the $N'_v = 3N_f$ since each triangle contains 3 vertices. Considering the average degree for a human designed regular mesh is 6, this implies each vertex is repeated 6 times. Therefore, we have the following approximate relationship: $N'_v \approx 6N_v$. Further, we have $N_v \approx 0.5N_f$.

Notice we utilize 4 tokens to compress a vertex, meaning the token length is around $4N_v$. Hence the compression ratio can be calculated as follows:

$$\frac{4N_v}{9N_f} \approx \frac{4 \cdot 0.5N_f}{9N_f} = 2/9$$

D.2 Derivation of average degree.

In a triangular mesh with many faces, the average vertex degree is closely related to the Euler characteristic [33; 27; 10]. The following derivation explains why the average degree approaches 6 in a high-quality triangular mesh with many faces.

1. Euler's Formula

For any planar graph or closed surface, Euler's formula is given by³:

$$V - E + F = \chi$$

where:

- V : Number of vertices,
- E : Number of edges,

³https://en.wikipedia.org/wiki/Euler_characteristic

- F : Number of faces,
- χ : Euler characteristic ($\chi = 2$ for planar graphs).

In our method, the meshes are processed as manifold structure, and its topology can be regarded as a planar graph, with each edge is shared by only two faces.

2. Relationship Between Faces and Edges in a Triangular Mesh

In the manifold triangular mesh, each face has 3 edges, and each edge is shared by two faces. Therefore, the total number of edges E is related to the number of faces F as:

$$E = \frac{3F}{2}$$

3. Average Vertex Degree

The degree of a vertex is defined as the number of edges connected to it. The average vertex degree AvgDegree for the entire mesh is:

$$\text{AvgDegree} = \frac{2E}{V}$$

where $2E$ represents each edge has two vertices. In addition, the degree of a vertex can also be considered as the ratio of the number of vertices without deduplication ($2E$) to the number of vertices with deduplication (V). Substituting $E = \frac{3F}{2}$ into the equation, we get:

$$\text{AvgDegree} = \frac{2 \cdot \frac{3F}{2}}{V} = \frac{3F}{V}$$

4. Substituting Euler's Formula

From Euler's formula, substituting $E = \frac{3F}{2}$, we can express V in terms of F :

$$V - \frac{3F}{2} + F = 2$$

Simplifying:

$$V = \frac{F}{2} + 2$$

5. Approaching the Limit

Substituting $V = \frac{F}{2} + 2$ into the equation for AvgDegree, we have:

$$\text{AvgDegree} = \frac{3F}{V} = \frac{3F}{\frac{F}{2} + 2}$$

As the number of faces F becomes very large (i.e., as the mesh is refined), the term $\frac{F}{2} + 2 \approx \frac{F}{2}$. Therefore:

$$\text{AvgDegree} \approx 6$$

This result demonstrates in a well-designed triangular mesh, the average vertex degree approaches 6.

E Image Conditioned and Text Conditioned Generation

For text-conditioned generation, we firstly utilize the Luma AI Genie⁴ text-to-3D model to generate dense meshes from text prompts, then we sample around 4096 point clouds to conduct point cloud conditioned generation for our auto-regressive model. For image-conditioned generation, we utilize TRELLIS [40] for image-to-3D generation, and sample 4096 point clouds for our model too. Fig. 21 and Fig. 22 demonstrate our high-quality and well-aligned results.

⁴<https://lumalabs.ai/genie>




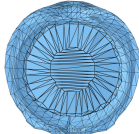

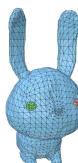
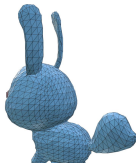
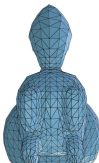


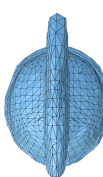


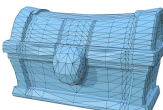
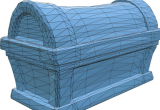
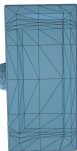

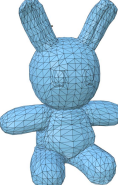
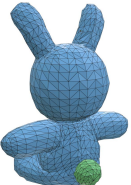
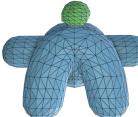

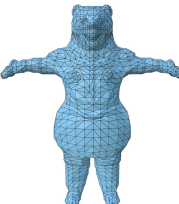
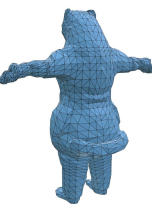
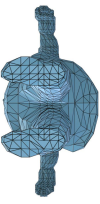
| Text Prompt | 2D image | Generated | | | |
|---|---|--|---|---|--|
| <i>Stylized fantasy health potion</i> |  |  |  |  | |
| <i>Mini bunny, floppy ears, adorable</i> |  |  |  |  | |
| <i>Black gladiator helmet</i> |  |  |  |  | |
| <i>A stylize chest</i> |  |  |  |  | |
| <i>A plushy bunny</i> |  |  |  |  | |
| <i>A DSLR photo of a bear dressed in medieval armor</i> |  |  |  |  | |

Figure 21: Illustration of our text conditioned generation. The Luma AI Genie text-to-3D model is utilized to generate dense meshes from text prompts, then the point clouds are sampled for point clouds conditioned generation.



Figure 22: Illustration of our image conditioned generation. The TRELLIS [40] is utilized for image-to-3D generation and point clouds of dense mesh are sampled for point clouds conditioned generation.

F More Implementation Details

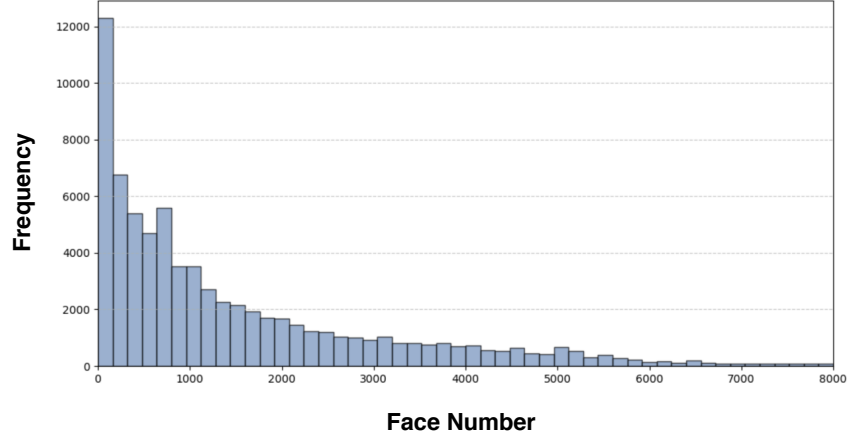


Figure 23: Illustration of the long-tail distribution of training data. The meshes with fewer faces constitute a larger proportion. Directly employing instance-balanced sampling may hinder the model’s ability to effectively learn from meshes with a higher number of faces.

Progressive-balanced Sampling. As illustrated in Fig. 23, our training data follows a long-tail distribution, hence we utilize progressive-balanced sampling in [14]. In early stages of training, we employ instance-balanced sampling until the loss decreases to 0.37 with around 100 epochs. In the following 200 epochs, we control the transition from instance-balanced sampling to class-balanced sampling with training progress ratio from 0 to 1. The final converging loss is around 0.25.

Data Augmentation. To increase data diversity, we apply following augmentation: (1) Scaling: Each axis of mesh is scaled randomly with a factor chosen from the range $[0.75, 0.95]$. (2) Rotation: The mesh is set to perform rotational augmentation around the y -axis, with each unit being 30 degrees, covering a total of 360 degrees. For point clouds sampling, we sample 4096 points from each mesh as condition and added gaussian noise to enhance robustness with probability 0.5 during training.

NeurIPS Paper Checklist

The checklist is designed to encourage best practices for responsible machine learning research, addressing issues of reproducibility, transparency, research ethics, and societal impact. Do not remove the checklist: **The papers not including the checklist will be desk rejected.** The checklist should follow the references and follow the (optional) supplemental material. The checklist does NOT count towards the page limit.

Please read the checklist guidelines carefully for information on how to answer these questions. For each question in the checklist:

- You should answer [Yes], [No], or [NA].
- [NA] means either that the question is Not Applicable for that particular paper or the relevant information is Not Available.
- Please provide a short (1–2 sentence) justification right after your answer (even for NA).

The checklist answers are an integral part of your paper submission. They are visible to the reviewers, area chairs, senior area chairs, and ethics reviewers. You will be asked to also include it (after eventual revisions) with the final version of your paper, and its final version will be published with the paper.

The reviewers of your paper will be asked to use the checklist as one of the factors in their evaluation. While "[Yes]" is generally preferable to "[No]", it is perfectly acceptable to answer "[No]" provided a proper justification is given (e.g., "error bars are not reported because it would be too computationally expensive" or "we were unable to find the license for the dataset we used"). In general, answering "[No]" or "[NA]" is not grounds for rejection. While the questions are phrased in a binary way, we acknowledge that the true answer is often more nuanced, so please just use your best judgment and write a justification to elaborate. All supporting evidence can appear either in the main paper or the supplemental material, provided in appendix. If you answer [Yes] to a question, in the justification please point to the section(s) where related material for the question can be found.

IMPORTANT, please:

- **Delete this instruction block, but keep the section heading "NeurIPS Paper Checklist",**
- **Keep the checklist subsection headings, questions/answers and guidelines below.**
- **Do not modify the questions and only use the provided macros for your answers.**

1. Claims

Question: Do the main claims made in the abstract and introduction accurately reflect the paper's contributions and scope?

Answer: [Yes]

Justification: The abstract and introduction clearly outline our paper's contributions, including a new mesh representation designed for auto-regressive model with several good geometric qualities. More details are listed at the end of Sec. Introduction.

Guidelines:

- The answer NA means that the abstract and introduction do not include the claims made in the paper.
- The abstract and/or introduction should clearly state the claims made, including the contributions made in the paper and important assumptions and limitations. A No or NA answer to this question will not be perceived well by the reviewers.
- The claims made should match theoretical and experimental results, and reflect how much the results can be expected to generalize to other settings.
- It is fine to include aspirational goals as motivation as long as it is clear that these goals are not attained by the paper.

2. Limitations

Question: Does the paper discuss the limitations of the work performed by the authors?

Answer: [Yes]

Justification: We list some limitations of our method at Sec. Conclusion.

Guidelines:

- The answer NA means that the paper has no limitation while the answer No means that the paper has limitations, but those are not discussed in the paper.
- The authors are encouraged to create a separate "Limitations" section in their paper.
- The paper should point out any strong assumptions and how robust the results are to violations of these assumptions (e.g., independence assumptions, noiseless settings, model well-specification, asymptotic approximations only holding locally). The authors should reflect on how these assumptions might be violated in practice and what the implications would be.
- The authors should reflect on the scope of the claims made, e.g., if the approach was only tested on a few datasets or with a few runs. In general, empirical results often depend on implicit assumptions, which should be articulated.
- The authors should reflect on the factors that influence the performance of the approach. For example, a facial recognition algorithm may perform poorly when image resolution is low or images are taken in low lighting. Or a speech-to-text system might not be used reliably to provide closed captions for online lectures because it fails to handle technical jargon.
- The authors should discuss the computational efficiency of the proposed algorithms and how they scale with dataset size.
- If applicable, the authors should discuss possible limitations of their approach to address problems of privacy and fairness.
- While the authors might fear that complete honesty about limitations might be used by reviewers as grounds for rejection, a worse outcome might be that reviewers discover limitations that aren't acknowledged in the paper. The authors should use their best judgment and recognize that individual actions in favor of transparency play an important role in developing norms that preserve the integrity of the community. Reviewers will be specifically instructed to not penalize honesty concerning limitations.

3. Theory assumptions and proofs

Question: For each theoretical result, does the paper provide the full set of assumptions and a complete (and correct) proof?

Answer: [\[Yes\]](#)

Justification: We provided the full set of assumptions and complete proof in main text and appendix.

Guidelines:

- The answer NA means that the paper does not include theoretical results.
- All the theorems, formulas, and proofs in the paper should be numbered and cross-referenced.
- All assumptions should be clearly stated or referenced in the statement of any theorems.
- The proofs can either appear in the main paper or the supplemental material, but if they appear in the supplemental material, the authors are encouraged to provide a short proof sketch to provide intuition.
- Inversely, any informal proof provided in the core of the paper should be complemented by formal proofs provided in appendix or supplemental material.
- Theorems and Lemmas that the proof relies upon should be properly referenced.

4. Experimental result reproducibility

Question: Does the paper fully disclose all the information needed to reproduce the main experimental results of the paper to the extent that it affects the main claims and/or conclusions of the paper (regardless of whether the code and data are provided or not)?

Answer: [\[Yes\]](#)

Justification: All the details are provided in the Sec. Experiments and Appendix to reproduce our results.

Guidelines:

- The answer NA means that the paper does not include experiments.
- If the paper includes experiments, a No answer to this question will not be perceived well by the reviewers: Making the paper reproducible is important, regardless of whether the code and data are provided or not.
- If the contribution is a dataset and/or model, the authors should describe the steps taken to make their results reproducible or verifiable.
- Depending on the contribution, reproducibility can be accomplished in various ways. For example, if the contribution is a novel architecture, describing the architecture fully might suffice, or if the contribution is a specific model and empirical evaluation, it may be necessary to either make it possible for others to replicate the model with the same dataset, or provide access to the model. In general, releasing code and data is often one good way to accomplish this, but reproducibility can also be provided via detailed instructions for how to replicate the results, access to a hosted model (e.g., in the case of a large language model), releasing of a model checkpoint, or other means that are appropriate to the research performed.
- While NeurIPS does not require releasing code, the conference does require all submissions to provide some reasonable avenue for reproducibility, which may depend on the nature of the contribution. For example
 - (a) If the contribution is primarily a new algorithm, the paper should make it clear how to reproduce that algorithm.
 - (b) If the contribution is primarily a new model architecture, the paper should describe the architecture clearly and fully.
 - (c) If the contribution is a new model (e.g., a large language model), then there should either be a way to access this model for reproducing the results or a way to reproduce the model (e.g., with an open-source dataset or instructions for how to construct the dataset).
 - (d) We recognize that reproducibility may be tricky in some cases, in which case authors are welcome to describe the particular way they provide for reproducibility. In the case of closed-source models, it may be that access to the model is limited in some way (e.g., to registered users), but it should be possible for other researchers to have some path to reproducing or verifying the results.

5. Open access to data and code

Question: Does the paper provide open access to the data and code, with sufficient instructions to faithfully reproduce the main experimental results, as described in supplemental material?

Answer: [Yes]

Justification: The data used for paper is public available. The training code, checkpoint, data preparation guidance will be released to public soon.

Guidelines:

- The answer NA means that paper does not include experiments requiring code.
- Please see the NeurIPS code and data submission guidelines (<https://nips.cc/public/guides/CodeSubmissionPolicy>) for more details.
- While we encourage the release of code and data, we understand that this might not be possible, so “No” is an acceptable answer. Papers cannot be rejected simply for not including code, unless this is central to the contribution (e.g., for a new open-source benchmark).
- The instructions should contain the exact command and environment needed to run to reproduce the results. See the NeurIPS code and data submission guidelines (<https://nips.cc/public/guides/CodeSubmissionPolicy>) for more details.
- The authors should provide instructions on data access and preparation, including how to access the raw data, preprocessed data, intermediate data, and generated data, etc.
- The authors should provide scripts to reproduce all experimental results for the new proposed method and baselines. If only a subset of experiments are reproducible, they should state which ones are omitted from the script and why.

- At submission time, to preserve anonymity, the authors should release anonymized versions (if applicable).
- Providing as much information as possible in supplemental material (appended to the paper) is recommended, but including URLs to data and code is permitted.

6. Experimental setting/details

Question: Does the paper specify all the training and test details (e.g., data splits, hyper-parameters, how they were chosen, type of optimizer, etc.) necessary to understand the results?

Answer: [\[Yes\]](#)

Justification: We provided all of the details in Sec. Experiments and Appendix.

Guidelines:

- The answer NA means that the paper does not include experiments.
- The experimental setting should be presented in the core of the paper to a level of detail that is necessary to appreciate the results and make sense of them.
- The full details can be provided either with the code, in appendix, or as supplemental material.

7. Experiment statistical significance

Question: Does the paper report error bars suitably and correctly defined or other appropriate information about the statistical significance of the experiments?

Answer: [\[Yes\]](#)

Justification: The paper reports CD, HD, NC and INCI, which are commonly used as a measure of performance of mesh quality. This approach is standard in the field and is sufficient to convey the performance of methods under investigation.

Guidelines:

- The answer NA means that the paper does not include experiments.
- The authors should answer "Yes" if the results are accompanied by error bars, confidence intervals, or statistical significance tests, at least for the experiments that support the main claims of the paper.
- The factors of variability that the error bars are capturing should be clearly stated (for example, train/test split, initialization, random drawing of some parameter, or overall run with given experimental conditions).
- The method for calculating the error bars should be explained (closed form formula, call to a library function, bootstrap, etc.)
- The assumptions made should be given (e.g., Normally distributed errors).
- It should be clear whether the error bar is the standard deviation or the standard error of the mean.
- It is OK to report 1-sigma error bars, but one should state it. The authors should preferably report a 2-sigma error bar than state that they have a 96% CI, if the hypothesis of Normality of errors is not verified.
- For asymmetric distributions, the authors should be careful not to show in tables or figures symmetric error bars that would yield results that are out of range (e.g. negative error rates).
- If error bars are reported in tables or plots, The authors should explain in the text how they were calculated and reference the corresponding figures or tables in the text.

8. Experiments compute resources

Question: For each experiment, does the paper provide sufficient information on the computer resources (type of compute workers, memory, time of execution) needed to reproduce the experiments?

Answer: [\[Yes\]](#)

Justification: We provided the computer resources at Sec Experiments.

Guidelines:

- The answer NA means that the paper does not include experiments.
- The paper should indicate the type of compute workers CPU or GPU, internal cluster, or cloud provider, including relevant memory and storage.
- The paper should provide the amount of compute required for each of the individual experimental runs as well as estimate the total compute.
- The paper should disclose whether the full research project required more compute than the experiments reported in the paper (e.g., preliminary or failed experiments that didn't make it into the paper).

9. Code of ethics

Question: Does the research conducted in the paper conform, in every respect, with the NeurIPS Code of Ethics <https://neurips.cc/public/EthicsGuidelines>?

Answer: [Yes]

Justification: The research adheres to the code of ethics.

Guidelines:

- The answer NA means that the authors have not reviewed the NeurIPS Code of Ethics.
- If the authors answer No, they should explain the special circumstances that require a deviation from the Code of Ethics.
- The authors should make sure to preserve anonymity (e.g., if there is a special consideration due to laws or regulations in their jurisdiction).

10. Broader impacts

Question: Does the paper discuss both potential positive societal impacts and negative societal impacts of the work performed?

Answer: [Yes]

Justification: The paper discussed this in Sec. Introduction and Sec. Conclusion.

Guidelines:

- The answer NA means that there is no societal impact of the work performed.
- If the authors answer NA or No, they should explain why their work has no societal impact or why the paper does not address societal impact.
- Examples of negative societal impacts include potential malicious or unintended uses (e.g., disinformation, generating fake profiles, surveillance), fairness considerations (e.g., deployment of technologies that could make decisions that unfairly impact specific groups), privacy considerations, and security considerations.
- The conference expects that many papers will be foundational research and not tied to particular applications, let alone deployments. However, if there is a direct path to any negative applications, the authors should point it out. For example, it is legitimate to point out that an improvement in the quality of generative models could be used to generate deepfakes for disinformation. On the other hand, it is not needed to point out that a generic algorithm for optimizing neural networks could enable people to train models that generate Deepfakes faster.
- The authors should consider possible harms that could arise when the technology is being used as intended and functioning correctly, harms that could arise when the technology is being used as intended but gives incorrect results, and harms following from (intentional or unintentional) misuse of the technology.
- If there are negative societal impacts, the authors could also discuss possible mitigation strategies (e.g., gated release of models, providing defenses in addition to attacks, mechanisms for monitoring misuse, mechanisms to monitor how a system learns from feedback over time, improving the efficiency and accessibility of ML).

11. Safeguards

Question: Does the paper describe safeguards that have been put in place for responsible release of data or models that have a high risk for misuse (e.g., pretrained language models, image generators, or scraped datasets)?

Answer: [NA]

Justification: The paper does not release any data or models that are considered to have a risk for misuse.

Guidelines:

- The answer NA means that the paper poses no such risks.
- Released models that have a high risk for misuse or dual-use should be released with necessary safeguards to allow for controlled use of the model, for example by requiring that users adhere to usage guidelines or restrictions to access the model or implementing safety filters.
- Datasets that have been scraped from the Internet could pose safety risks. The authors should describe how they avoided releasing unsafe images.
- We recognize that providing effective safeguards is challenging, and many papers do not require this, but we encourage authors to take this into account and make a best faith effort.

12. Licenses for existing assets

Question: Are the creators or original owners of assets (e.g., code, data, models), used in the paper, properly credited and are the license and terms of use explicitly mentioned and properly respected?

Answer: [Yes]

Justification: All existing assets used in the paper are properly credited, and their licenses and terms of use are explicitly respected.

Guidelines:

- The answer NA means that the paper does not use existing assets.
- The authors should cite the original paper that produced the code package or dataset.
- The authors should state which version of the asset is used and, if possible, include a URL.
- The name of the license (e.g., CC-BY 4.0) should be included for each asset.
- For scraped data from a particular source (e.g., website), the copyright and terms of service of that source should be provided.
- If assets are released, the license, copyright information, and terms of use in the package should be provided. For popular datasets, paperswithcode.com/datasets has curated licenses for some datasets. Their licensing guide can help determine the license of a dataset.
- For existing datasets that are re-packaged, both the original license and the license of the derived asset (if it has changed) should be provided.
- If this information is not available online, the authors are encouraged to reach out to the asset's creators.

13. New assets

Question: Are new assets introduced in the paper well documented and is the documentation provided alongside the assets?

Answer: [NA]

Justification: The paper does not introduce any new assets.

Guidelines:

- The answer NA means that the paper does not release new assets.
- Researchers should communicate the details of the dataset/code/model as part of their submissions via structured templates. This includes details about training, license, limitations, etc.
- The paper should discuss whether and how consent was obtained from people whose asset is used.
- At submission time, remember to anonymize your assets (if applicable). You can either create an anonymized URL or include an anonymized zip file.

14. Crowdsourcing and research with human subjects

Question: For crowdsourcing experiments and research with human subjects, does the paper include the full text of instructions given to participants and screenshots, if applicable, as well as details about compensation (if any)?

Answer: [NA]

Justification: The paper does not involve crowdsourcing experiments or research with human subjects.

Guidelines:

- The answer NA means that the paper does not involve crowdsourcing nor research with human subjects.
- Including this information in the supplemental material is fine, but if the main contribution of the paper involves human subjects, then as much detail as possible should be included in the main paper.
- According to the NeurIPS Code of Ethics, workers involved in data collection, curation, or other labor should be paid at least the minimum wage in the country of the data collector.

15. **Institutional review board (IRB) approvals or equivalent for research with human subjects**

Question: Does the paper describe potential risks incurred by study participants, whether such risks were disclosed to the subjects, and whether Institutional Review Board (IRB) approvals (or an equivalent approval/review based on the requirements of your country or institution) were obtained?

Answer: [NA]

Justification: The paper does not involve research with human subjects.

Guidelines:

- The answer NA means that the paper does not involve crowdsourcing nor research with human subjects.
- Depending on the country in which research is conducted, IRB approval (or equivalent) may be required for any human subjects research. If you obtained IRB approval, you should clearly state this in the paper.
- We recognize that the procedures for this may vary significantly between institutions and locations, and we expect authors to adhere to the NeurIPS Code of Ethics and the guidelines for their institution.
- For initial submissions, do not include any information that would break anonymity (if applicable), such as the institution conducting the review.

16. **Declaration of LLM usage**

Question: Does the paper describe the usage of LLMs if it is an important, original, or non-standard component of the core methods in this research? Note that if the LLM is used only for writing, editing, or formatting purposes and does not impact the core methodology, scientific rigor, or originality of the research, declaration is not required.

Answer: [NA]

Justification: The paper does not involve LLMs as any important, original, or non-standard components.

Guidelines:

- The answer NA means that the core method development in this research does not involve LLMs as any important, original, or non-standard components.
- Please refer to our LLM policy (<https://neurips.cc/Conferences/2025/LLM>) for what should or should not be described.